Copernicus Marine Service

QUALITY INFORMATION DOCUMENT

Black Sea MFC
BLKSEA_ANALYSISFORECAST_WAV_007_003

Issue: 3.1

Contributors: Joanna Staneva, Marcel Ricker, Arno Behrens

Approval date by the CMEMS product quality coordination team: 22/11/2022

CHANGE RECORD

When the quality of the products changes, the QuID is updated and a row is added to this table. The third column specifies which sections or sub-sections have been updated. The fourth column should mention the version of the product to which the change applies.

Issue	Date	§	Description of Change	Author	Validated By
1.0	08/01/2018	All	First version of the document of CMEMS V4	A. Behrens, J. Staneva, G. Gayer	E. Peneva
1.1	26/03/2018	All	Minor corrections by Mercator after V4 review	F. Hernandez	F. Hernandez
1.2	22/02/2019	All	Adapting the description of the forecasting system from 5 to 10 days forecast release	J. Staneva	
2.0	25/09/2020	All	Complete revision due to new model version	J. Staneva, A. Behrens, G. Gayer, M. Ricker	E. Peneva
3.0	25/09/2021	All	Complete revision due to new model version and new resolution	J. Staneva, M. Ricker, A. Behrens	E. Peneva
3.1	29/11/2022	All	Addition of data assimilation into the system and update of source terms	J. Staneva, M. Ricker, A. Behrens	E. Peneva

TABLE OF CONTENTS

I EXECUTIVE SUMMARY

I.1 Products covered by this document

This document describes the quality of the analysis and forecast nominal product of the wave component of the Black Sea: BLKSEA_ANALYSISFORECAST_WAV_007_003. The product includes the following 2D 1-hourly analysis and forecast instantaneous fields:

- VHMO: spectral significant wave height (Hm0);
- VTM10: spectral moments (-1,0) wave period (Tm-10);
- VTM02: spectral moments (0,2) wave period (Tm02);
- VTPK: wave period at spectral peak / peak period (Tp);
- VMDR: mean wave direction from (Mdir);
- VPED: wave principal direction at spectral peak;
- VSDX: stokes drift U;
- VSDY: stokes drift V;
- VHM0_WW: spectral significant wind wave height;
- VTM01_WW: spectral moments (0,1) wind wave period;
- VMDR_SW1: mean wind wave direction from;
- VHM0_SW1: spectral significant primary swell wave height;
- VTM01_SW1: spectral moments (0,1) primary swell wave period;
- VMDR_SW1: mean primary swell wave direction from;
- VHM0_SW2: spectral significant secondary swell wave height;
- VTM01_SW2: spectral moments (0,1) secondary swell wave period;
- VMDR_SW2: mean secondary swell wave direction from;
- VZMX: maximum zero crossing wave height (Hmax); and
- VTMX: maximum wave period (Tmax).

The output data are produced at 1/40°x1/40° horizontal resolution.

I.2 Summary of the results

The quality of the hindcast component of the new EAS5 Black Sea MFC wave system used to produce the BLKSEA_ANALYSISFORECAST_WAV_007_003 product has been accessed via comparison against satellite observations recorded by the radar altimeters of the satellites Sentinel-3a, Sentinel-3b, Cryosat-2, Jason-3, SARAL/Altika, CFOSat, and Sentinel-6 (the latter satellite has been added compared to the previous QUID) for the time period 01/05/2021 to 30/04/2022. In addition, coastal regions have been validated by using wave buoy data. The horizontal spatial grid resolution of the BS-waves model is 1/40° in the zonal and 1/40° in meridional direction (ca. 2.5 km). The assessment of the corresponding wave hindcast is the best way of understanding the validity of the WAM model since the wave analysis-forecast system provided to CMEMS are done by taking into account surface currents and water level deviations from the hydrodynamic model (BLKSEA_ANALYSISFORECAST_PHY_007_001). The ocean model data are interpolated to the WAM model grid. The growth of errors in the wave forecasts is dominated by growth errors in the forcing fields, which are the U_{10} wind fields from the IFS010 (Integrated Forecasting System) of the ECMWF with 1/10°x1/10° spatial resolution. As the wind is the

most important forcing of the wave model, satellite-derived wind speed is compared to the IFS010 wind speed. Satellite winds are available from February 2020 ongoing. Compared to the previous system, the new system includes data assimilation of satellite significant wave height measurements (satellites included in WAVE_GLO_WAV_L3_SWH_NRT_OBSERVATIONS_014_001).

The main results of the BLKSEA_ANALYSISFORECAST_WAV_007_003 quality product assessment are summarised below:

Significant wave height from altimeter: Comparisons of the significant wave heights (SWH) have been done with satellite altimeter data obtained by the satellites Sentinel-3a, Sentinel-3b, Cryosat-2, SARAL/Altika, Jason-3, CFOSat, and Sentinel-6a. The BS-waves NRT system presents good accuracy in terms of the SWH. The model skill enhancement based on different statistical parameters compared to the old product is evident. The SWH of the wave model and observations are correlated at a level higher than 0.95. In general, the wave model tends to slightly overestimate the satellite measurements. The bias is mostly negative with values between 5 and 11 cm. It is noted that buoy data is only available from stations close to the coast whereas satellite altimeter measurements are expected to have relatively high errors in these coastal regions. This limits the direct comparison of satellite and buoy data.

Wave Buoy validations: In the period May 2020 to April 2022 time series of eleven buoys (SPOT0772, SPOT0773, SPOT0776, WAVEB01, WAVEB02, WAVEB03, WAVEB04, WAVEB05, WAVEB06, WD3044, Gelendzhik) were available (INSITU_BS_NRT_OBSERVATIONS_013_034). The water depth at the buoy locations is often shallow (17 m/20 m) and the wave buoys are located close to the coast. The quality control of some of the stations is still insufficient, which limits the validations against in-situ observations. Nevertheless, the modelled significant wave height shows a good correlation with buoy data. In addition to SWH, the in-situ observations provide other wave parameters, such as maximum wave height, mean direction, peak direction, T_{M02} period, and peak period. The correlation between the model and buoy data for these parameters is also very good. Some peaks of the SWH in the time series are slightly underestimated compared to in-situ observations. Reasons for this could be the vicinity of the coast, the model resolution or deviations in the bathymetry from the real water depth. The enhancement of the model skill compared to the previous model version is mainly visible as improved peaks of the significant wave height. As the buoys are located in coastal Black Sea regions, this finding is consistent with the along-track altimeter validations. The skill improvements are due to (i) better model configuration: finer spatial resolution of the wave model than the previous version, improved Black Sea bathymetry; (ii) new high-resolution wind forcing; (iii) new wave model physics.

I.3 Estimated Accuracy Numbers

Estimated Accuracy Numbers (EANs) for the results of the BS-waves system are the mean of the differences between computed and measured values (model minus observation) (bias) and the corresponding root mean square differences (RMSD).
EANs are computed for:

- Significant Wave Height: Refers to the "spectral significant wave height (VHM0)".

The observations are:

- Significant wave height: recorded by the radar altimeters of the satellites Sentinel-3a, Sentinel-3b, Cryosat-2, Jason-3, SARAL/Altika, CFOSat, and Sentinel-6), which additionally include wind speed measurements.
- Significant wave height: recorded by the available wave buoys for the considered period.

The EANS computed for the EAS5 version of the CMEMS Black Sea wave modelling system are based on the simulation of the system in hindcast mode for a two-year period between May 2020 and April 2022, which will replace the old dataset. Section VI presents comparisons with the previous NRTsetup. The final values for bias and RMSD for the individual satellites are given in Table 1.

Since the bias is the difference model mean minus mean of the measurements, the EANs for the BS-wave system indicate in general a small overestimation of the measurements by the wave model between 5 and 11 cm. The RMSD varies between 11 and 24 cm. The smallest bias (5 cm) can be detected for Sentinel-3a, Sentinel-3b, and CFOSat, whereas the highest biases (and RMSD) emerge from the satellites Sentinel-6a, which was recently introduced in CMEMS and, so far, provides only a few measurements.

When merging all available satellite data, the bias is 6 cm and the RMSD 13 cm (Table 2), which is considered a good model performance. As in this new setup, the EANs in Tables 1 and 2 now depend on the model itself, and new EANs of independent measurement (wave buoys) are introduced.

Table 3 shows a bias of 12 cm and an RMSD of 21 cm for the merged data of all available buoys. Both numbers are a bit higher than for the satellites and reveal a slight overestimation of significant wave height in coastal regions.

*Table 1: Significant wave height EANs **from the different satellites** for the NRT BS-waves system (all values in centimetres).*

Period: May 2020 to April 2022		
Satellite (Abr.)	Bias [cm]	RMSD [cm]
SARAL/Altika (Al)	6	11
Cryosat-2 (C2)	8	12
Jason-3 (J3)	7	12
Sentinel-3a (S3a)	5	13
Sentinel-3b (S3b)	5	14
CFOSat (CFO)	5	12
Sentinel-6a (S6a)	11	24

*Table 2: Significant wave height EANs **from satellites** for the NRT BS-waves system (all values in centimetres).*

Period: May 2020 to April 2022		
Satellite (Abr.)	Bias [cm]	RMSD [cm]
All satellites (All merged)	6	13

*Table 3: Significant wave height EANs **from buoys** for the NRT BS-waves system (all values in centimetres).*

Period: May 2020 to April 2022		
Buoy (Abr.)	Bias [cm]	RMSD [cm]
All buoys (All buoys)	12	21

II PRODUCTION SYSTEM DESCRIPTION

II.1 Production centre details

Production centre name: Helmholtz-Zentrum Hereon (former HZG), Germany

Production system name: Black Sea Waves Analysis and Forecast

Available variables (2D):

- VHMO: spectral significant wave height (Hm0);
- VTM10: spectral moments (-1,0) wave period (Tm-10);
- VTM02: spectral moments (0,2) wave period (Tm02);
- VTPK: wave period at spectral peak / peak period (Tp);
- VMDR: mean wave direction from (Mdir);
- VPED: wave principal direction at spectral peak;
- VSDX: stokes drift U;
- VSDY: stokes drift V;
- VHM0_WW: spectral significant wind wave height;
- VTM01_WW: spectral moments (0,1) wind wave period;
- VMDR_SW1: mean wind wave direction from;
- VHM0_SW1: spectral significant primary swell wave height;
- VTM01_SW1: spectral moments (0,1) primary swell wave period;
- VMDR_SW1: mean primary swell wave direction from;
- VHM0_SW2: spectral significant secondary swell wave height;
- VTM01_SW2: spectral moments (0,1) secondary swell wave period;
- VMDR_SW2: mean secondary swell wave direction from;
- VZMX: maximum zero crossing wave height (Hmax); and
- VTMX: maximum wave period (Tmax).

Frequency of model output: Hourly instantaneous

Geographical coverage: 27.25°E → 42.00°E; 40.50°N → 47.00°N (the Azov Sea is excluded)

Horizontal resolution: 1/40° in zonal direction, 1/40° in meridional direction (ca. 2.5 km)

Vertical coverage: Surface only

Length of forecast: 10 days

Frequency of forecast release: Daily

Analyses: No

Hindcast: Yes (one day)

Frequency of hindcast release: Daily

Data assimilation: Yes, significant wave height and wind speed data from the satellites Sentinel-3a, Sentinel-3b, Cryosat-2, Jason-3, SARAL/Altika, CFOSat, and Sentinel-6 (WAVE_GLO_WAV_L3_SWH_NRT_OBSERVATIONS_014_001).

Citation (DOI): Staneva, J., Ricker, M., & Behrens, A. (2022). Black Sea Waves Analysis and Forecast (CMEMS BS-Waves, EAS5 system) (Version 1) [Data set]. Copernicus Monitoring Environment Marine Service (CMEMS). https://doi.org/10.25423/CMCC/BLKSEA_ANALYSISFORECAST_WAV_007_003_EAS5

The wave forecasts for the Black Sea are produced by the Hereon Production Unit utilizing the WAM wave model (described below).
The BS-waves system runs once per day starting at 23:30:00 pm local time. It produces 10-day (240 h) forecast fields initialised by a 1-day (24 h) hindcast.

The BS-waves system integration is composed of several steps:

1. Upstream data acquisition, pre-processing and control of: (i) ECWMF atmospheric model IFS010 (Integrated Forecasting System) provided by the ECMWF (European Centre for Medium-Range Weather Forecasts); (ii) satellite data (WAVE_GLO_WAV_L3_SWH_NRT_OBSERVATIONS_014_001); (iii) currents and water level deviations generated by the hydrodynamic model of the CMCC (BLKSEA_ANALYSISFORECAST_PHY_007_001).
2. Hindcast/Forecast: WAM produces one day of hindcast and 10 days of forecast.
3. Post-processing: the model output is processed to obtain the products for the CMEMS catalogue.
4. Output delivery.

The BLKSEA_ANALYSISFORECAST_WAV_007_003 production chain is represented in Figure 1.

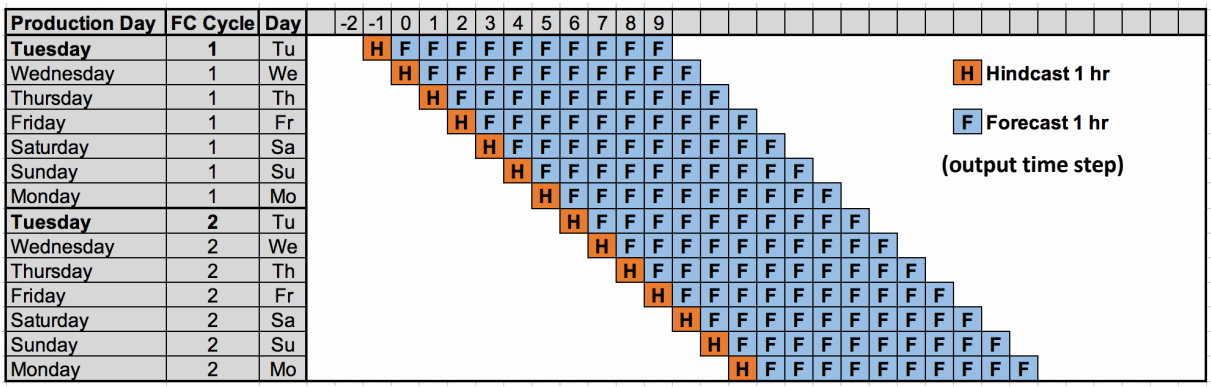

Figure 1: BS-WAV production chain.

II.2 System Description

This document details the quality of products from the Black Sea Wave Analysis and Forecast system. These products are generated using the WAM Cycle 6 Black Sea model (spatial resolution of about 2.5 km), which includes the most recent developments. The wave model considers ocean surface gravity wave (periods 1.5 to 24 seconds) characteristics as an extension to the existing physical and ecosystem model products provided by the Black Sea MFC. The following subsections describe the model components and their dependencies in terms of models providing the forcing.

Region, grid and bathymetry

The regional wave model for the semi-enclosed Black Sea runs in shallow water mode on a model grid situated between 27.25°E to 42.00°E and 40.50°N to 47.00°N, with a spatial resolution of about 2.5 km, (1/40° in latitude and longitude direction). The required bathymetry for the model grid is based upon the General Bathymetric Chart of the Oceans (GEBCO 2019 Grid, http://www.gebco.net) 30 sec data. The bathymetry is only a controlling mechanism on the wave field for depths below approximately 490 m, based on a minimum frequency in the model of 0.042 Hz (period 24 seconds). The model area and the corresponding depth distribution are shown in Figure 2.

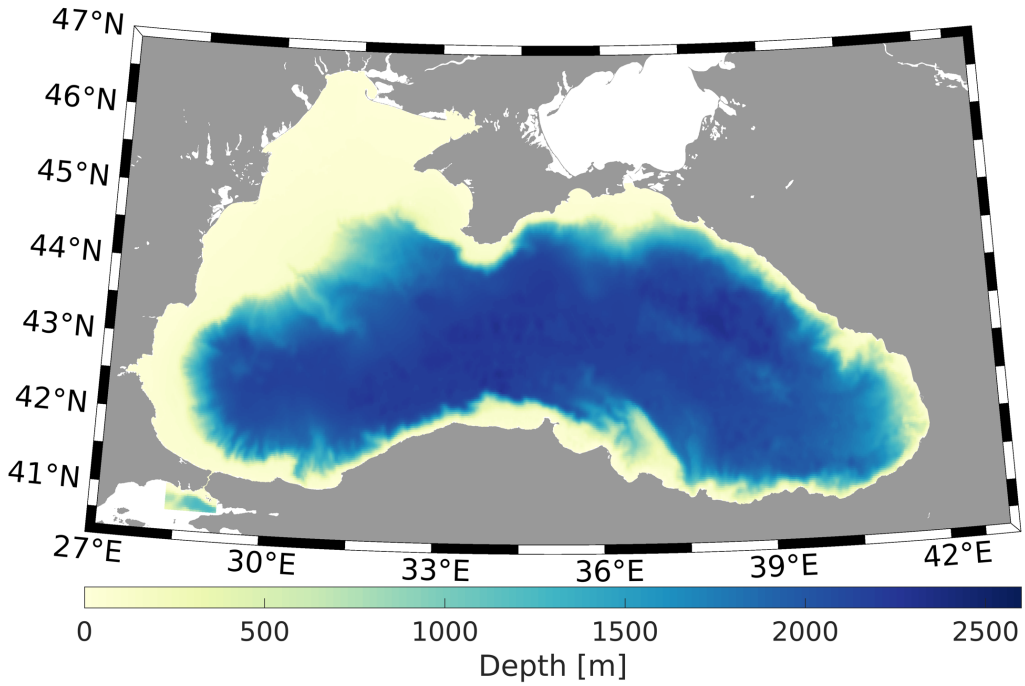

Figure 2: Black Sea wave model WAM bathymetry.

Spectral grid

WAM calculates the two-dimensional energy density spectrum at each of the 74,518 active model grid points in the frequency and directional space. The solution of the energy balance equation is provided for 24 directional bands at 15° each, starting at 7.5° and measured clockwise to true north, and 30 frequencies logarithmically spaced from 0.042 Hz to 0.663 Hz at intervals of $\Delta f/f = 0.1$. Therefore, the prognostic part of the wave model covers periods from approximately 23.8 to 1.5 seconds. To include the important contribution of higher frequency waves to wave growth/dissipation processes and for the output wave characteristics, a parametric tail is fitted for frequencies above the spectral maximum (e.g. WAMDI Group, 1988).

Wave model and source term physics configuration

The system BS-waves is based on the state-of-the-art and well-established advanced third-generation spectral wave model WAM that runs successfully at many

institutions worldwide. It is based on the spectral description of the wave conditions in frequency and directional space at each of the active model sea grid points of a certain model area. The energy balance equation, complemented with a suitable description of the relevant physical processes is used to follow the evolution of each wave spectral component. WAM computes the two-dimensional wave variance spectrum through the integration of the transport equation (1) in spherical coordinates (see also ECMWF (2020)):

$$\frac{\partial F}{\partial t} + (\cos\Phi)^{-1}\frac{\partial}{\partial\Phi}(\dot{\Phi}\cos\Phi F) + \frac{\partial}{\partial\lambda}(\dot{\lambda}F) + \sigma\frac{\partial}{\partial\sigma}\left(\dot{\sigma}\frac{F}{\sigma}\right) + \frac{\partial}{\partial\theta}(\dot{\theta}F) = S \qquad (1)$$

$$\dot{\Phi} = (c_g\cos\theta + u_{North})/R$$

$$\dot{\lambda} = (c_g\sin\theta + u_{East})/(R\cos\Phi)$$

$$\dot{\theta} = c_g\sin\theta\tan\Phi/\mathrm{R} + \dot{\theta}_D + \dot{\theta}_C$$

$$\dot{\sigma} = \dot{\sigma}_C$$

with,

$\mathrm{F}(\lambda,\Phi,\sigma,\theta,\mathrm{t})$	wave energy density spectrum
(λ,Φ)	longitude, latitude
(σ,θ)	intrinsic frequency, wave direction

The first term of (1) describes the local rate of change of energy density in time, the second and third ones the propagation in geographical space, the fourth one the shifting of the relative frequency due to variations in depths and currents and the last one on the left side of the equation the contribution of the depth- and current-induced refraction. The source functions on the right of the transport equation comprise the contributions of wind input (S_{in}), nonlinear interaction (S_{nl}), dissipation (S_{dis}), bottom friction (S_{bf}) and wave breaking (S_{br}):

$$\mathrm{S} = S_{in} + S_{nl} + S_{dis} + S_{bf} + S_{br}$$

A detailed description is given by the WAMDI Group (1988), Komen et al. (1994), Günther et al. (1992), and Janssen (2008). The WAM Cycle 6 that is used for the Black Sea wave hindcast is an update of the former WAM Cycle 4. The basic physics and numerics are kept in that new release. The source function integration scheme made by Ardhuin et al. (2010) is incorporated. The wave model performance has been discussed in Stanev et al. (2014), Staneva et al. (2015; 2016a,b), Wahle et al. (2015), and in the recent Ocean State Reports #4 & #5 (von Schuckmann et al., 2020, 2021). Wave breaking has been taken into account. WAM Cycle 6.0 contains model physics that is similar to what is described by Ardhuin et al. (2010) and is often referred to as “Source term package 4" (ST4), but with some differences described by Breivik et al. (2021) The ST4 physics package was implemented into the WAM code in the frame of

the CMEMS Service Evolution project WAVEFLOW (CONSISTENT WAVE-MEAN FLOW MODELLING IN COUPLED MODELS), (https://www.mercator-ocean.eu/en/portfolio/waveflow/).

Data assimilation

Assimilation of satellite significant wave height measurements into the wave fields is incorporated in this system using the sequential optimal interpolation scheme. In total, L3 along-track data of seven satellites are used.

In contrast to the previous NRT system, the assimilation of measured satellite data has been taken into account. The required radar altimeter data for that purpose is available on the CMEMS server and includes, besides significant wave height, wind speed L3 data as well. The measured data will be assimilated into the wave model fields by the use of a sequential optimal interpolation scheme. The advantage of sequential methods in contrast to variational methods is the relative simplicity and the relatively small amount of required computational resources. The disadvantage is the fact that the significant wave height is not a dynamical quantity in the wave model, but only an output parameter derived from the spectrum. Therefore the procedure is split into two steps: first, the SWH and wind speed data are used to construct analysed fields of SWH and wind speed by the OI and the second step consists of the reconstruction of the spectrum from the analysed fields. Since the wave model generates one-hourly output, the time of the satellite track can differ between 0 and 30 minutes from the nearest neighbour of the model grid points in time. The spatial error can be half of the mesh size of the spatial resolution of the model which is about 1.25 km. Quality control is included in the model so that unreasonable values are discarded automatically. Satellites cross the Black Sea once or twice a day in less than two minutes, so very few measured values are available for assimilation into the wave and wind fields. Taking that into account and since the waves are propagating fast and have therefore a very small memory at that regional scale, we expect no significant influence of the assimilation on the wave model results. For the new NRT system, all radar altimeter measurements of the CMEMS satellites that were available have been assimilated: Sentinel-3a, Sentinel-3b, Cryosat-2, Jason-3, SARAL/Altika, CFOSat, and Sentinel-6 (WAVE_GLO_WAV_L3_SWH_NRT_OBSERVATIONS_014_001).

Forcing

The driving forces for the wave model are the U_{10} wind fields provided by the atmospheric model IFS010 (Integrated Forecasting System; https://www.ecmwf.int/en/forecasts/datasets/set-i) of the ECMWF (European Centre for Medium-Range Weather Forecasts) via the CMCC server. The temporal resolution of the wind forcing is 6-h for the 24-h hindcast, 1-h for the first 3 days of the forecast, 3-h hourly for the next 3 days, and 6-h for the rest of the forecast cycle. The spatial resolution of the IFS010 data is about 10 km (1/10°x1/10°). Boundary values are not required since the Black Sea is a semi-enclosed area. The wave model is additionally forced by the Black Sea PHY NRT data (BLKSEA_ANALYSISFORECAST_PHY_007_001). Hourly time dependent depth and current fields from the BS-PHY NEMO model are taken into account.

Wave growth

The growth of waves under extratropical wind storms and tropical cyclones has been the topic of several studies in the past two decades (Powell et al., 2003; Donelan et al., 2004; Zweers et al., 2010; Chen et al., 2013). Wave growth is controlled by the aerodynamic roughness of the surface, i.e., the drag that is felt by the wind. There is increasing evidence from theoretical (Makin, 2005), laboratory (Donelan et al., 2004;) and field studies (Powell et al., 2003; Holthuijsen et al., 2012; Donelan, 2018) that the roughness (and thus the drag) starts to level or even drop (Powell et al., 2003) at very high wind speeds. Thus, how

wave models parameterize wave growth under high winds becomes increasingly important as forecast systems, both coupled and uncoupled, move towards higher resolution (Li et al., 2021, Breivik et al, 2022).

To reduce possible underestimates of satellite radar altimeter measurements by the wave model, the parameterisation of the wave growth in the wind input source term has been adapted to the driving wind fields. The source term for the wind input is: The wave growth is controlled by the wind input term Sin. The form used in WAM Cycle 6 is based on the formulation presented as Eq. (19) by Ardhuin et al. (2010):

$$S_{\mathrm{in}} = \frac{\rho_{\mathrm{a}}\beta_{\max}}{\rho_{\mathrm{w}}\kappa^2}\mathrm{e}^{Z}Z^4\left[\frac{u_*}{c}\right]^2 \max\left(\cos(\theta-\phi),0\right)^p \sigma F(k,\theta).$$

Here, F(k;) [m3 rad⁻1] is the wave variance density in wavenumber (k)-direction (ϑ) space, φ is the wind direction, β_{max} is a constant nondimensional growth parameter and

$$Z = \ln(k\, z_0) + \kappa/[\cos(\vartheta-\varphi)(u_*/c + z_\alpha)]$$

is an effective wave age with c the phase speed, the intrinsic circular frequency [rads-1] and z_0 a dimensionless wave age tuning parameter that shifts the growth curve. The directional spread is controlled by the power p, a tunable constant which is commonly (and here) set to 2. Higher powers give a more narrowly directed wind input.

It is important to note that Ardhuin et al. (2010) already introduced a cap on the surface roughness in the form

$$z_0 = \min(\alpha_0 u^2/g, z_{0,\max})$$

The growth rate, normalised by the angular frequency ω, derived from a parametrization by Janssen (1991) results from :

$$\frac{\gamma}{\omega} = \varepsilon\beta x^2$$

with ε the air-water density ratio, β the Miles parameter, and $x = \frac{u^*}{c}\max\left(\cos(\theta-\varphi),0\right)$.

The Miles parameter β depends again on a constant called β_m with a default value of 1.2 after Janssen (1991). Here the β_{max} parameter has been tuned to $\beta_{max} = 1.8$ for the Black Sea to enable stronger wave growth.

Initial conditions

The initial conditions of the wave model are constrained over successive cycles by including a 24-hour hindcast run of the model prior to each forecast. The role of the hindcast is to apply analysed wind fields to the wave model so that the model is forced by the best available descriptions of the atmosphere and ocean. This is an effective method of preventing any drift in wave model initial conditions since the key response in the wave model is to the wind and the use of analysed forcing fields reduces the impact of any systematic drifts in the atmospheric model. By the same token, wave model errors are generally anticipated to be dominated by errors in the wind field after approximately 24-36 hours forecast lead time, so the benefits from using assimilation to constraining initial condition errors are unlikely to hold for forecasts beyond days one to two ahead.

Partitioning method

Included in model outputs are characteristics describing individual wave components that make up a given sea-state. For example, a sea may consist simply of a single wind-sea component for which all wave energy is affected by the forcing wind, or multiple swell components, which have been remotely generated by distant storms. In WAM these components are determined using a two-stage process. Individual components are derived from the two-dimensional wave spectrum. This process effectively treats the wave spectrum as a topographic map from which individual peaks in wave energy can be identified to define the separate wave components.

The second part of the procedure follows an assumption that wind sea should be defined as only that part of the wave energy spectrum which is directly forced by the wind (this is an assumption, which is most regularly used by operational wave forecasters who wish to be able to reference the evolution of wind sea directly against evolution in the local wind conditions). Using this assumption, wave spectrum bins where wave speed is slower than the (co-directed) wind speed are associated with the wind sea component. The assignment of special energy to wind sea overrides any previous assignment of wave energy to the topographic components made in the first step.

III VALIDATION FRAMEWORK

To evaluate and assure the quality of the BLKSEA_ANALYSISFORECAST_WAV_007_003 product of the CMEMS BS-waves version EAS5, the system has been integrated into hindcast mode for the period from 01/05/2020 to 30/04/2022. All CMEMS satellite measurements that are available for the entire two-year time period (Sentinel-3a, Sentinel-3b, Cryosat-2, SARAL/Altika, Jason-3, CFOSat, and Sentinel-6a; WAVE_GLO_WAV_L3_SWH_NRT_OBSERVATIONS_014_001) have been used to compare the significant wave height with the corresponding wave model results. As a precondition to enable these comparisons, the satellite data has to be correlated with the wave model data in space and time. The corresponding satellites need up to two minutes only to cross the Black Sea and the measurements recorded by the radar altimeter have been compared with the computed results of the nearest model output time. For each of the individual measurements with its unambiguous assignment to longitude and latitude, always the computed values of the nearest model grid point in space have been used to compare.

Since the radar altimeter of the satellites measures wind speed (available from February 2020) and significant wave height, the only integrated wave parameter that can be used for validation is the significant wave height (SWH).

The measured data undergo quality control to make sure that unrealistic values are not taken into account. Such values can occur when the satellite passes the transition zone between land and sea at the coasts. Usually, the satellites pass the Black Sea once a day, sometimes twice.

Although in-situ wave measurements from moored wave buoys are available from CMEMS In-Situ Thematic Assemble Centre (CMEMS INS TAC) (INSITU_BS_NRT_OBSERVATIONS_013_034) for the Black Sea, their locations are restricted to coastal areas of the southwestern basin. The corresponding water depths are mostly 17 m or 20 m and in the model domain, these positions are located at the land-sea boundary or only a few grids in the ocean. As the wave parameters are very sensitive to the water depth, the buoy positions in the model were slightly shifted (1-2 grids) in order to place them at a more realistic water depth. Time series at these grids have been used for validation.

Periods with obvious buoy measurement errors were detected and excluded from the validations. Further information about the Black Sea buoy data quality is currently not available but we established a collaboration with INS TAC to report measurement issues. This information will be used to, in turn, further improve the quality of the INS TAC data.

dWe also refer to our operational validation provided on a monthly basis to the CMEMS Product Quality Dashboard (https://pqd.mercator-ocean.fr/). Here, daily metrics are presented, which also include forecast skills.

III.1 Statistical analysis

We present scatter plots that show measured against modelled significant wave heights for each of the satellites separately. We also consider the case, in which all the measurements are combined without distinguishing between satellites.

We illustrate overplotting (as there thousands pairs of measured and modelled data) by estimating the bi-variate probability density by evaluating a 2d-Gaussian kernel on a square grid in the variable space.

Furthermore, the plots include summary statistics, such as the mean value and standard deviation, and statistics that describe the skill of WAM to simulate the significant wave heights.

The skill scores used are Pearson's product-moment correlation coefficient (Corr), the root mean squared difference (RMSD), the bias, and the scatter index (SI). The scores read as follows, where o and m stand for observed and modelled data. An overbar over a variable denotes the temporal average value derived from the sample of length n.

$$Correlation = \frac{\frac{1}{n-1}\sum_{i=1}^{n}(o_i - \bar{o})(m_i - \bar{m})}{\sqrt{\frac{1}{n-1}\sum_{i=1}^{n}(o_i - \bar{o})^2}\sqrt{\frac{1}{n-1}\sum_{i=1}^{n}(m_i - \bar{m})^2}}$$

$$RMSD \sqrt{\frac{1}{n}\sum_{i=1}^{n}(m_i - o_i)^2}$$

$$bias = \frac{1}{n}\sum_{i=1}^{n}(m_i - o_i)$$

$$SI = \frac{\sqrt{\frac{1}{n-1}\sum_{i=1}^{n}(m_i - o_i - BIAS)^2}}{\bar{o}}$$

One of the general assumptions for the correlation coefficient is that variables follow a normal distribution, which is not the case for the significant wave height. It might be advisable to use another measure to gauge the monotonic relation between modelled and observed significant wave heights, such as the rank correlation. However, we use Pearson's correlation coefficient as it is a quasi-standard for evaluating numerical models. Note that the skill metric RV is an adaptation of the Brier Skill Score and gauges the error variance (assuming a zero-mean error) against the variance of observations. RV is bound by $-\infty$ and one. While the latter stands for perfect model skill, negative values would indicate no skill at all. As the error variance, here expressed as the sum of squared errors, can be decomposed into components related to the standard deviations and the correlation coefficient, RV not only depends on the magnitude of errors, but also on the capability of WAM to simulate the temporal variability of the wave fields.

The scatter plots also show the least-squares linear fit without including any intercept between measurements and modelling results. Ideally, such a fit would be close to the straight line dividing the scatter plot at an angle of 45°, which is included as a reference.

Last, we also show pairs of quantiles of the measured and modelled significant wave heights. The quantiles are estimated from the empirical cumulative density function at specific percentiles. The highest quantile shown, corresponds to the sampled maximum value, which translates to the 100th percentile of the empirical distribution.

IV VALIDATION RESULTS

IV.1 Along-track validations

The comparisons between the radar altimeter measurements and the model results have been done for the different satellite tracks that are available for the considered 2-year period. Since the wave heights in the Black Sea are usually moderate and the differences between measured and computed data are small in those cases, several interesting situations of that period are discussed here. Figure 3 shows two examples for comparisons of the computed significant wave height with Cryosat-2 and CFOSat data. It includes the distribution of SWH combined with a track of the satellite (upper panels) and the corresponding time series of measured and modelled wave height along the satellite tracks (lower panels). On the left side, it is the descending path on 11/03/2021 09:56:32 – 09:57:24 UTC, that touches the area of maximum wave height of about 3.7 m. The second example describes the conditions for the ascending path on 15/12/2021 16:31:15 – 16:32:27 UTC that crosses the area of maximum wave heights around 3.5 m. Both comparisons show a good agreement between satellite measurements and model results with a small underestimation by the model in the first example. Also, the lateral variability is well represented in both examples.

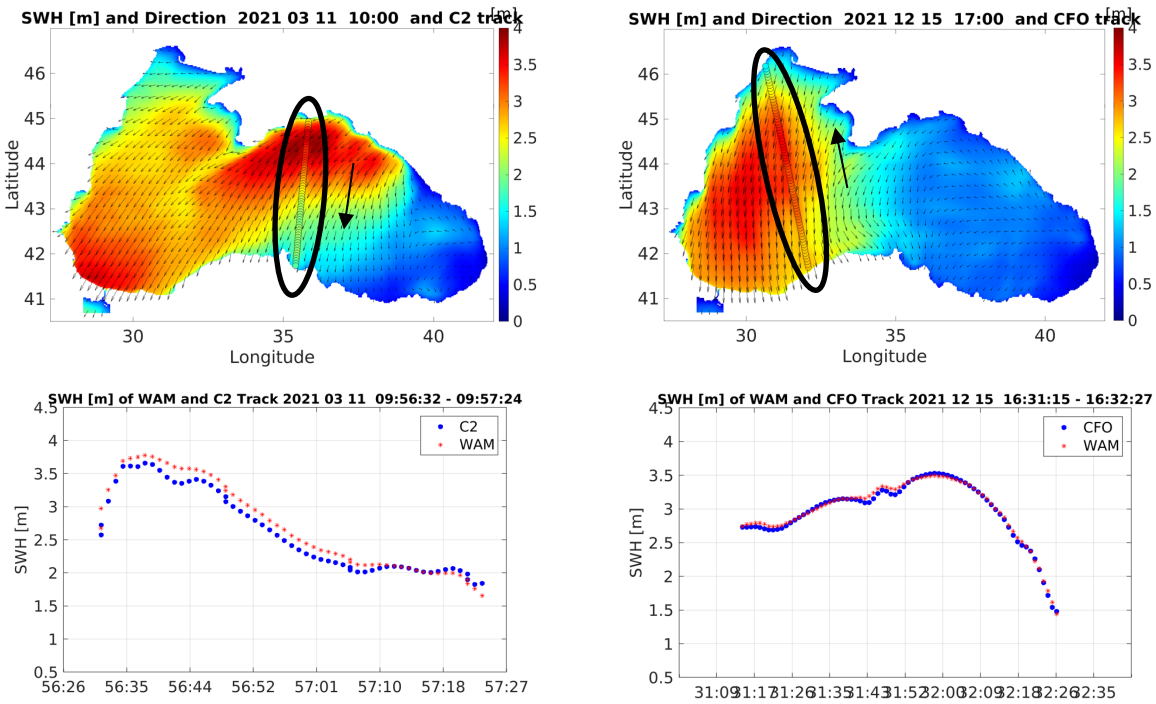

Figure 3: Left: distribution of significant wave height (SWH) on 11/03/2021 (10:00 UTC) and a Cryosat-2 satellite track 11/03/2021, 09:56:32 – 09:57:24 UTC. Right: distribution of SWH on 15/12/2021 (17:00 UTC) and a CFOSat satellite track 15/12/2021, 16:31:15 – 16:32:27 UTC. Solid black circles: locations of the tracks. The x-axis

Additionally, two examples for comparisons between wave model data and measurements, recorded by the radar altimeters of Sentinel-3a and Jason-3, are presented in Figure 4. The first example (left panels of Figure 4) shows an ascending track on 10/03/2022 19:35:56 – 19:36:32 UTC, that crosses a storm area with wave heights around 4 m in the south-west of the Black Sea. This satellite track is located close to the coast. The along-track validation (in the lower panel) demonstrates a good agreement during the whole satellite transit. Furthermore, the track also passes the domain in the Marmara Sea, where the performance is also good.

The second example (right panels of Figure 4) shows the descending path of the Jason-3 satellite on 01/12/2021 01:51:54 – 01:53:23 UTC that crosses an area with values of significant wave height up to 6.5 m, which are very high waves for the eastern basin. Even this extraordinary storm events have been simulated accurately with only slight overestimations during the first half of the track.

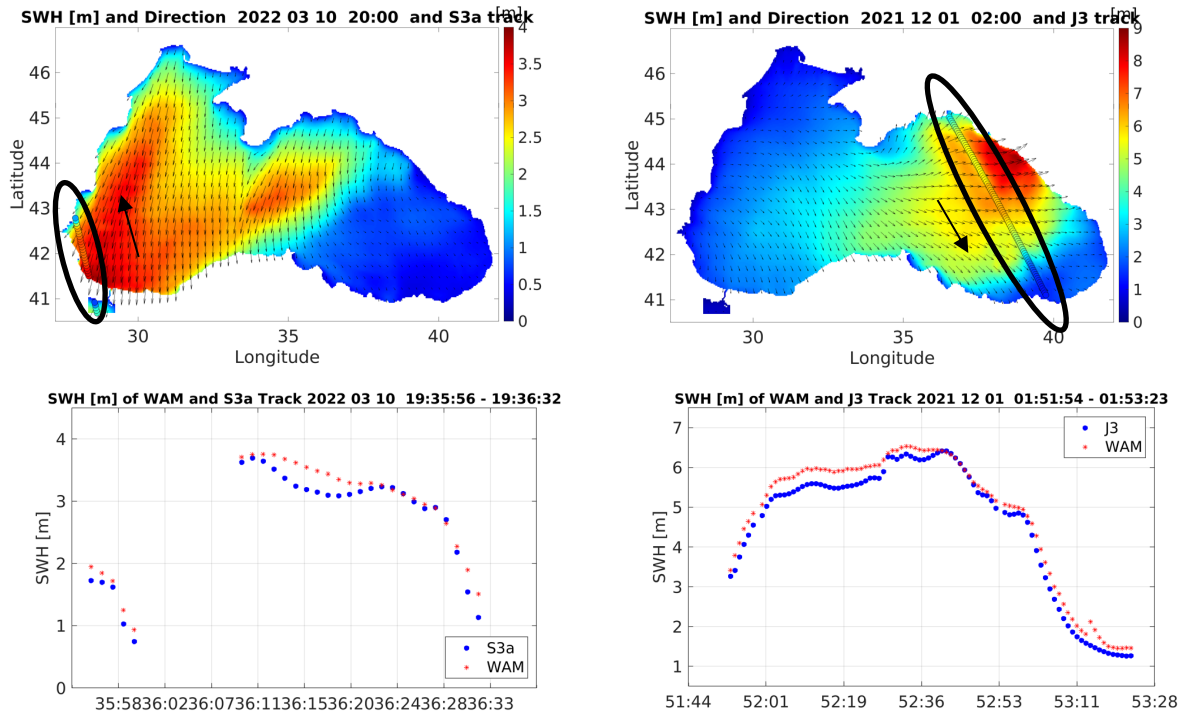

Figure 4: Left: distribution of significant wave height (SWH) on 10/03/2022 (20:00 UTC) and a Sentinel-3a satellite track 10/03/2022, 19:35:56 – 19:36:32 UTC. Right: distribution of SWH on 01/12/2021 (02:00 UTC) and a Jason-3 satellite track 01/12/2021, 01:51:54 – 01:53:23 UTC. Solid black circles: locations of the tracks. The x-axis represents time [hh:mm] of the day and hour given in the title. Arrows denote the satellite flight direction.

IV.2 Statistical analysis

Detailed statistics following the PQWG-Waves recommendations have been calculated for all comparisons between modelled and measured data recorded by the radar altimeter of the different satellites.

For the quarters of the considered time period (from May 2020 to April 2022), the analysis for the significant wave heights is presented as a QQ (Quantile-Quantile) -scatter plot including statistical parameters. These include the RMSD, bias, Scatter Index (SI), Pearson correlation coefficient (CORR), and best-fit Slope (SLOPE). The SI, defined here as the standard deviation of errors (model minus observations) relative to the observed mean of the significant wave, being dimensionless, is more appropriate to evaluate the relative closeness of the model output to the observations at different locations compared with the RMSD, which is representative of the size of a 'typical' error. The SLOPE corresponds to a best-fit line forced through the origin (zero intercepts). In addition to these core metrics, merged Density Scatter and Quantile-Quantile (QQ) plots are provided.

Concerning an overall validation procedure for the BS-waves system, the comparisons between all modelled and measured satellite data are analysed in detail for the full period from May 2020 to April 2022 (Figure 5, lower right). Representative results are also shown separately for the seven different satellites SARAL/Altika, Cryosat-2, Jason-3, Sentinel-3a, Sentinel-3b, CFOSat, and Sentinel-6a. In general, the statistics show a slight overestimation of the measured data ("R") by the wave model results ("M") occurring consistently among all satellites (bias ranges between 5 and 11 cm). The CORR is always above 0.95. The bias, RMSD, and CORR over all satellites are 6 cm, 13 cm, and 0.98, respectively (for the metrics see also Tables 1 and 2). This model performance of the new BS-WAV NRT data is considered to be good.

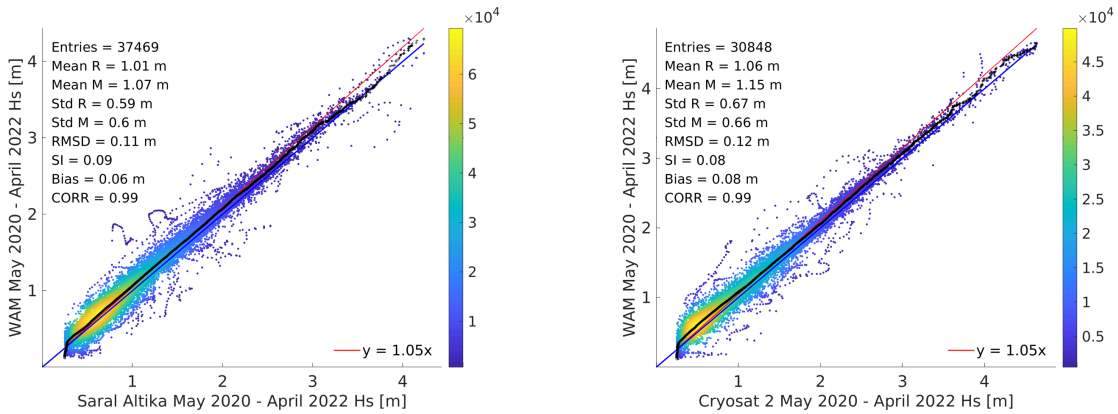

Figure 5: Scatter plots of significant wave height (Hs) for the 2-year period from May 2020 to April 2022 of 7 different satellites and the whole period using all satellites merged (lower right). See the labels for the satellite names. Also shown are the estimated bivariate probability density (coloured area), the linear slope-fit regression of modelled and observed wave heights (red line), specific quantiles taken from the empirical cumulative density function (black line), and the diagonal (blue line). Furthermore, summary statistics and skill scores are included. R: reference (satellite) data, M: model data (continues in next page).

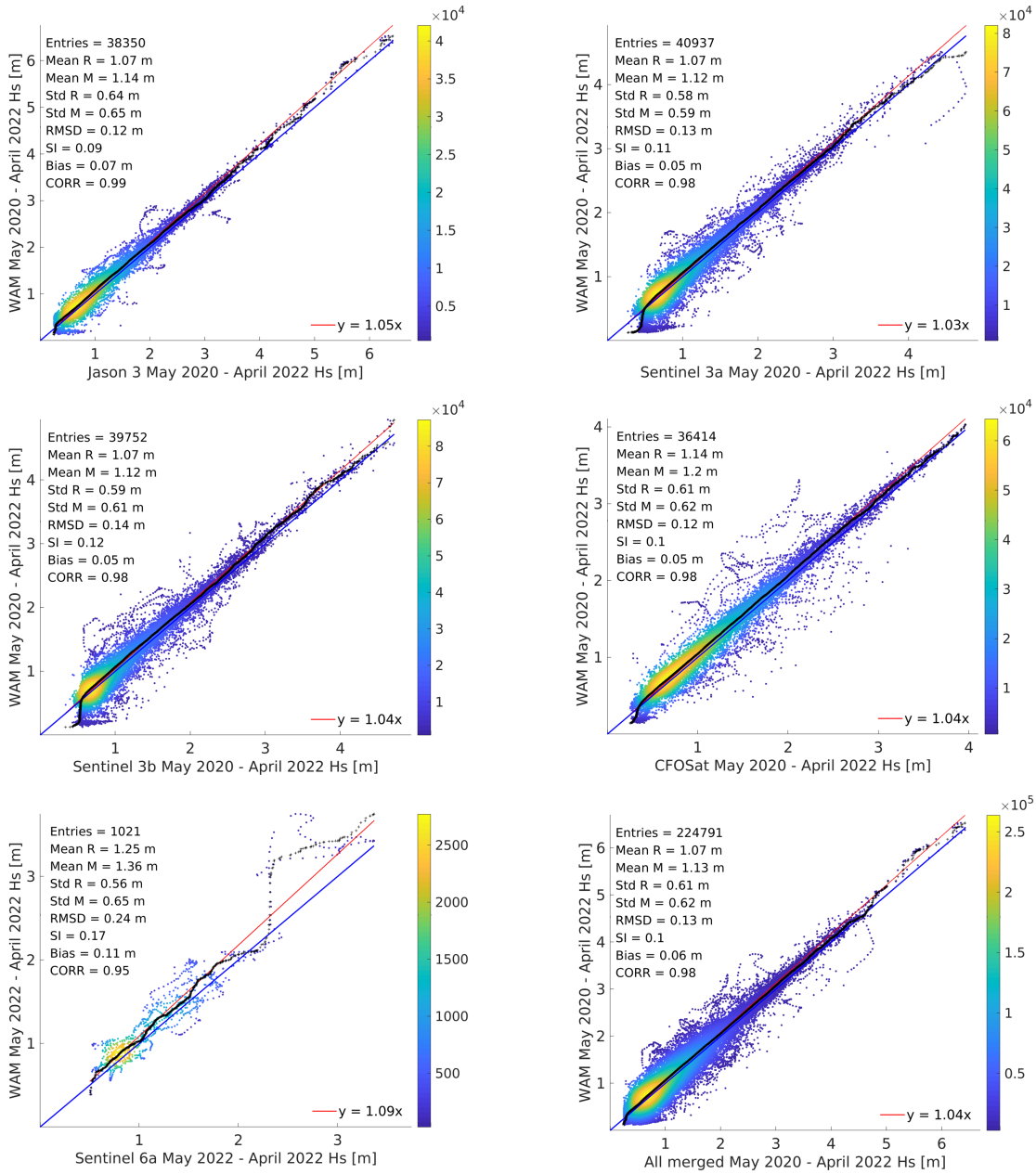

Figure 5: (continued)

Quarterly time series of the metrics (RMSD, bias, CORR, SI as well as the 99th and 99.9th percentiles of the differences between model and measurements) are presented in Figure 6. Seasonality of the differences is observed, in which the RMSD and percentiles show worse model performance (higher numbers) in winter than in summer. The RMSD, bias, CORR, and SI and mostly around 12 cm, 5 cm, 0.97, and 0.10, respectively. The differences among the single satellites are rather low. In general, the metrics can again be considered good.

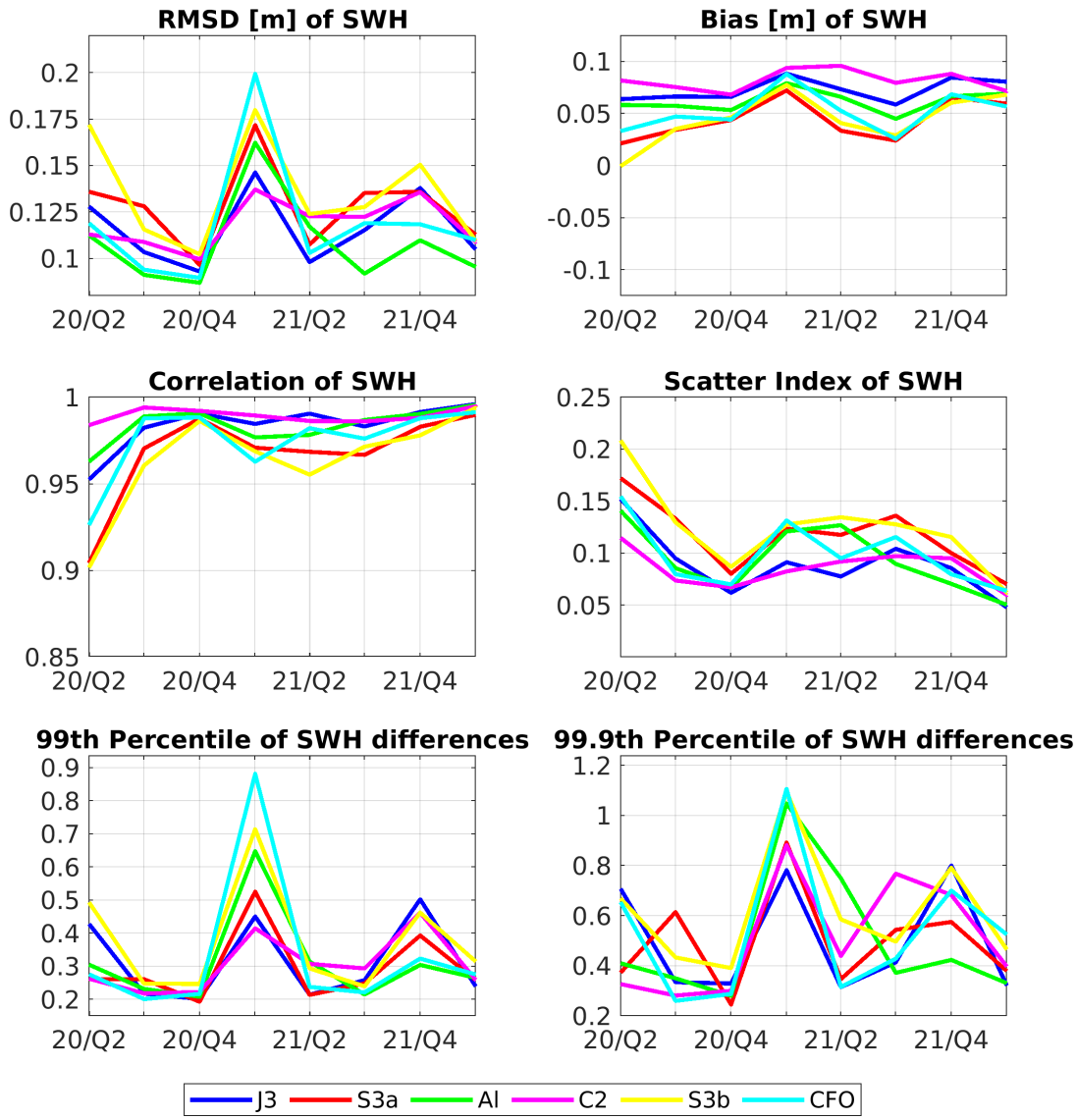

Figure 6: Quarterly comparisons of satellite and model significant wave height (SWH). The used satellites are: Jason-3 (J3), Sentinel-3a (S3a), SARAL/Altika (Al), Cryosat-2 (C2), Sentinel-3b (S3b), and CFOSat (CFO). The metrics are given in the titles.

IV.3 Buoy validations

The time period from May 2020 to April 2022 is (partly) covered by the time series of eleven wave buoys. Their locations and names are shown in Figure 7. The WAVEBXX and WD3044 buoys are mounted at a water depth of 17 m and the SPOTXXXX buoys at 20 m. They provide the variables significant wave height, maximum wave height, wave mean direction, wave peak direction, wave T_{M02} period, and wave peak period (however, not consistent among all buoys). For a visual demonstration of the model

performance, one buoy (WAVEB03) has been chosen and its results are presented in the following (Figure 8-14) as time series. The available buoy time series cover the 9-month period from July 2021 until March 2022.

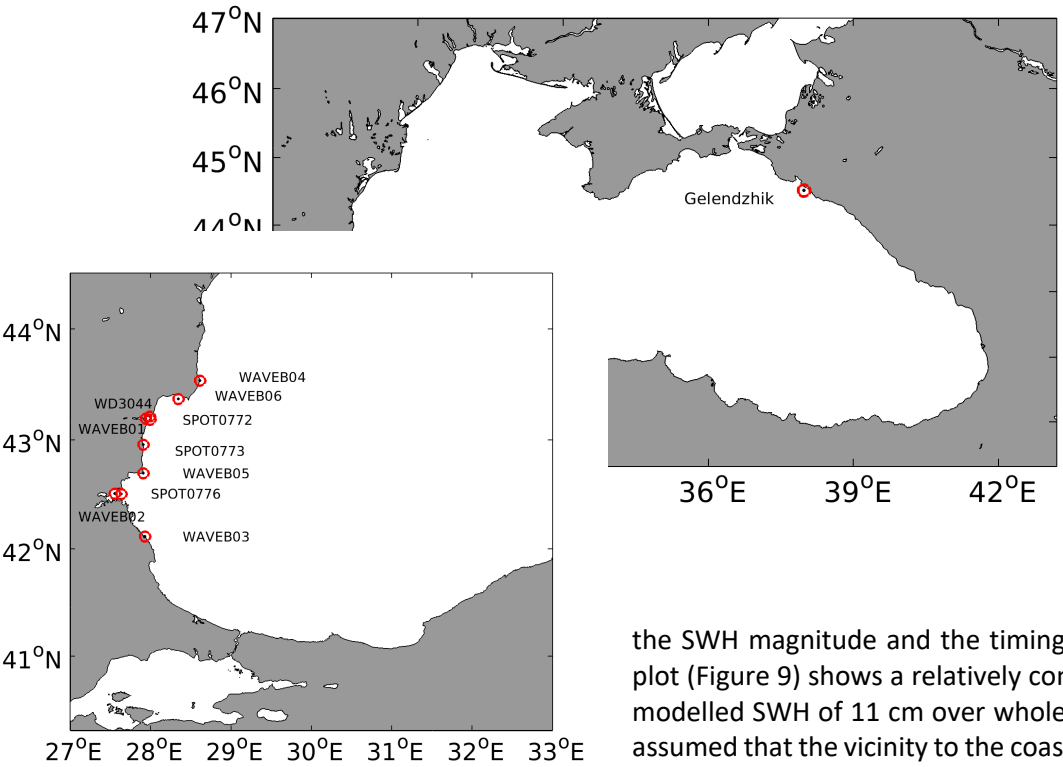

In the case of significant wave height, the model performs well over the whole 9 months (Figure 8). The performance is good in both, the SWH magnitude and the timing. The corresponding scatter plot (Figure 9) shows a relatively constant overestimation of the modelled SWH of 11 cm over whole range of wave heigths. It is assumed that the vicinity to the coast and probable uncertainties in the model bathymetry negatively influence such a comparison. Despite that, the overall metrics are still good with values of bias = 11 cm, RMSD = 21 cm, SI = 0.21, and CORR = 0.97.

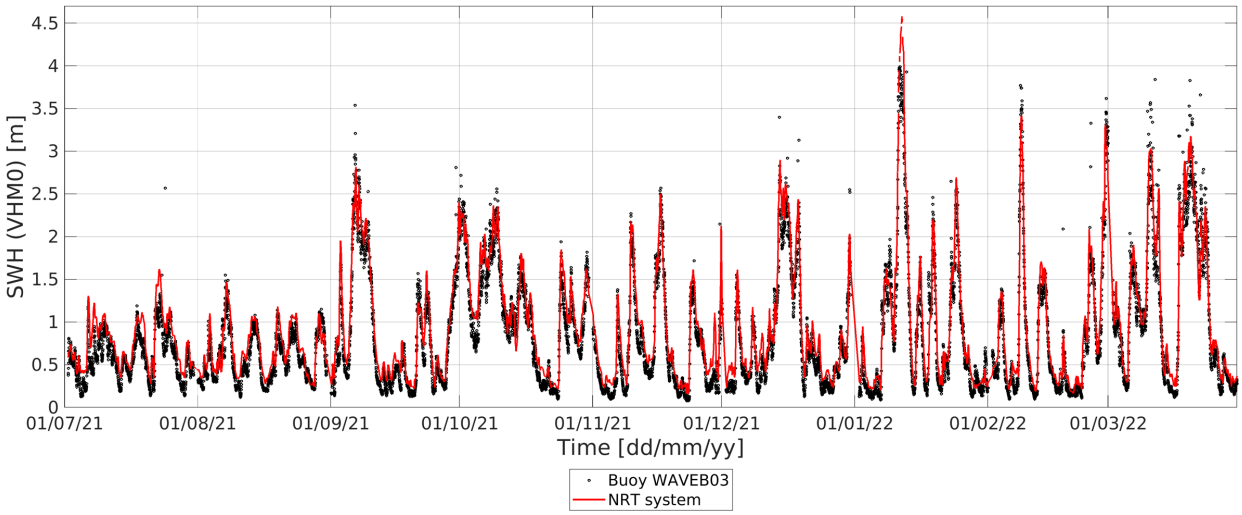

Figure 8: Significant wave height (VHM0) of the buoy WAVEB03 (all available data).

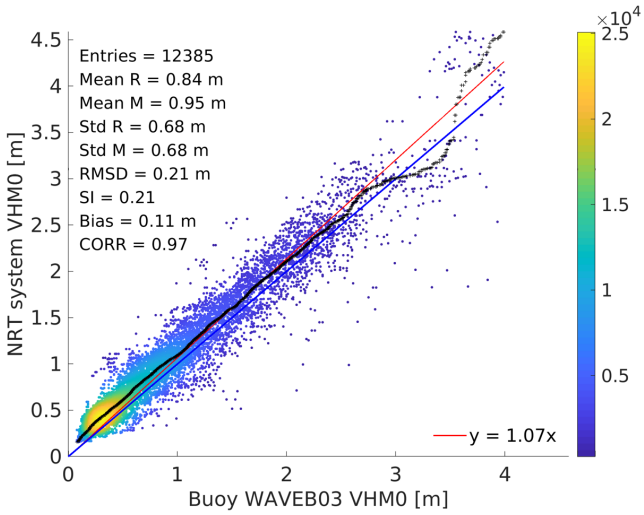

Figure 9: Scatter plot of significant wave height (VHM0) of the WAVEB03 buoy vs. model for the period shown in Figure 8. See Figure 5 for a detailed description of the scatter plot.

The availability of in-situ observations made it possible to perform validations not only for the SWH but also for other wave variables. The wave T_{M02} period (Figure 10) shows a similar behaviour then SWH. The timing is very good over the whole period but a slight overall underestimation is present. However, this underestimation is mostly less than 1 s (overall bias is -0.29 s), thus we can consider that the validations show good agreement against the observations for the T_{M02} period. It has to be noted that higher periods (higher than ~5 s) show a stronger deviation from the measurements (underestimated) than shorter periods.

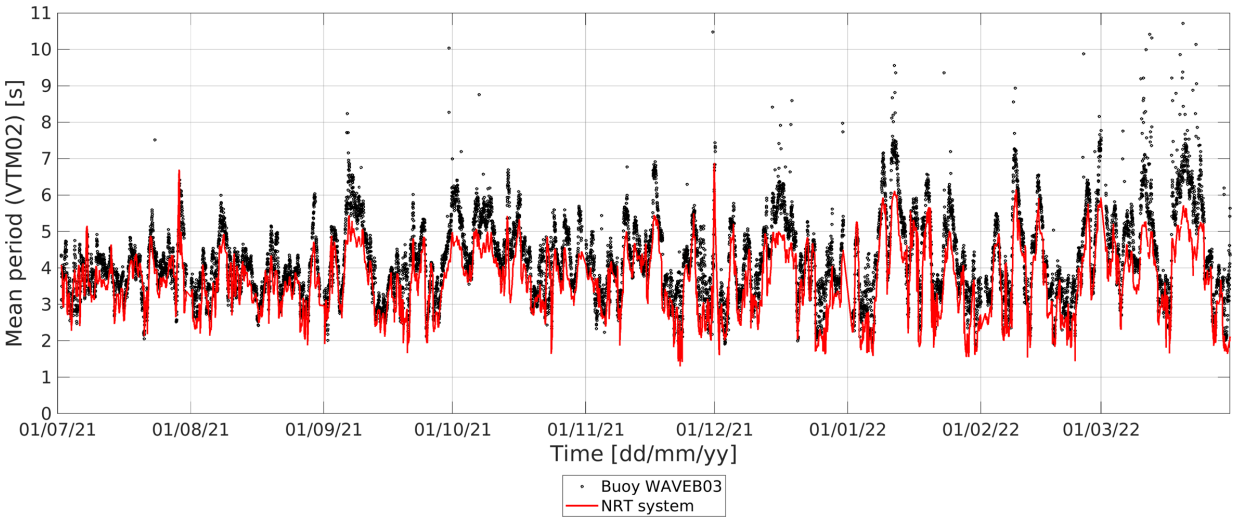

Figure 10: Wave T_{M02} period (VTM02) of the buoy WAVEB03 (all available data).

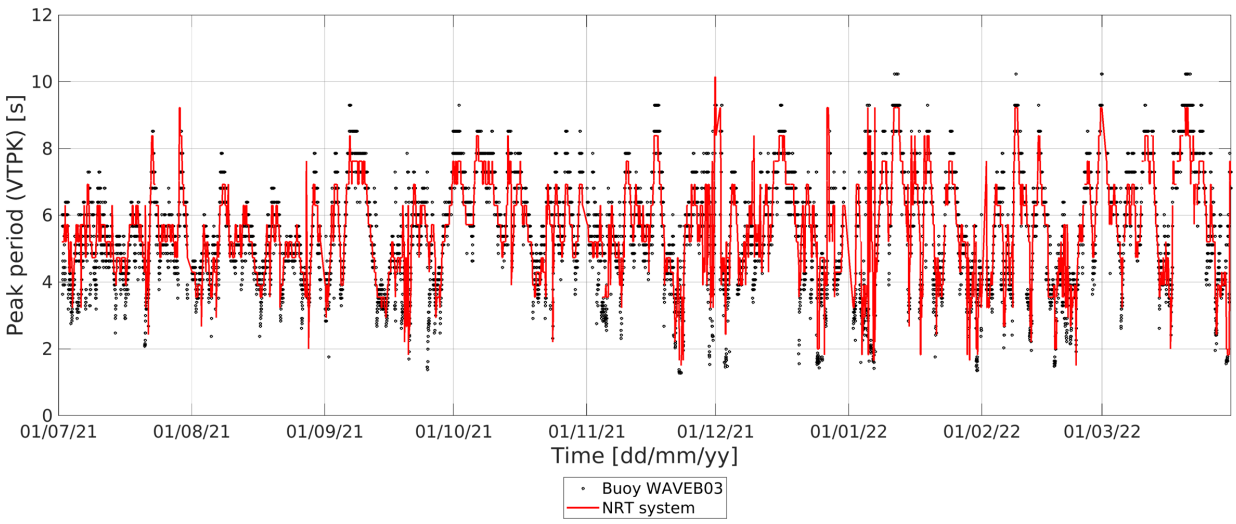

Figure 11: Wave peak period (VTPK) of the buoy WAVEB03 (all available data).

In contrast, the peak period is less underestimated (Figure 11) and the model performance of this variable is even better (overall bias is 0.02 s).

The simulated wave mean direction matches well with the in-situ data (Figure 12). Also, the short-term variations are well captured by the model. This good performance could be related to both the improved resolution of the wind forcing and the wave model. The performance of the wave peak direction (Figure 13) is comparable to the wave mean direction.

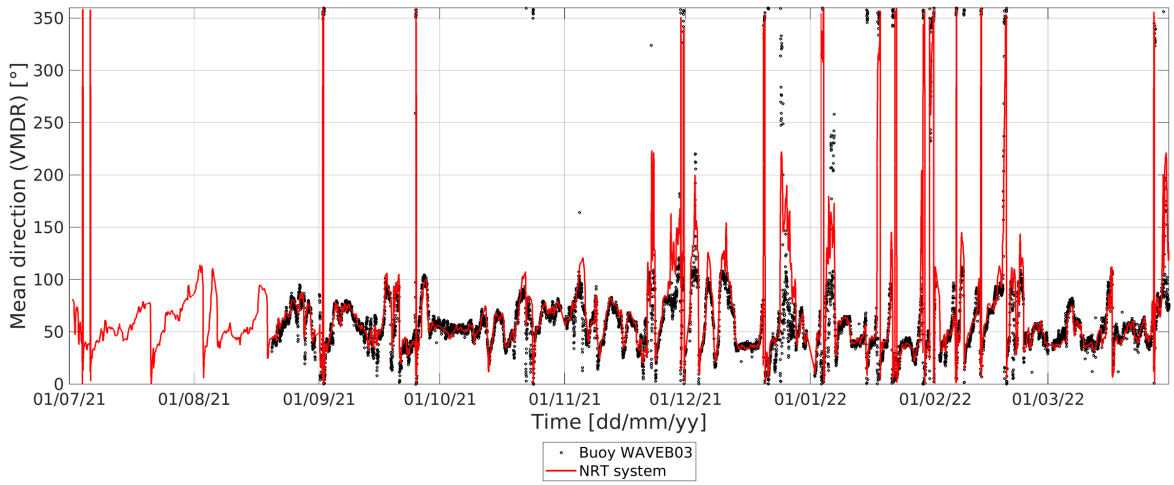

Figure 12: Wave mean direction (VMDR) of the buoy WAVEB03 (all available data). Vertical red lines appear due to the change from 359 to 0°.

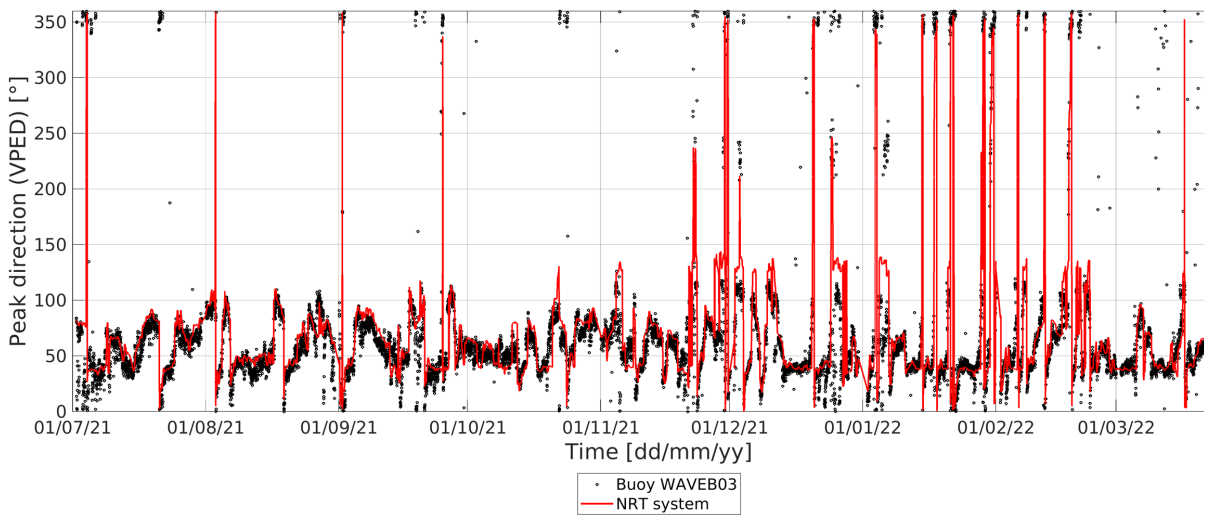

Figure 13: Wave peak direction (VPED) of the buoy WAVEB03 (all available data). Vertical red lines appear due to the change from 359 to 0°.

The buoy WAVEB03 does not provide maximum wave height data. Thus, the results of the buoy WAVEB01 are used instead (Figure 14) to demonstrate the model performance of the wave variable VZMX. The buoy WAVEB01 is located further north in the Gulf of Varna (see Figure 7).

Compared to the significant wave height, the timing of Hmax is slightly worse. In addition, the maximum wave height simulation is also worse in terms of amplitudes, which could be due to the different type/location of the buoy. However, the overall model performance can still be considered as good.

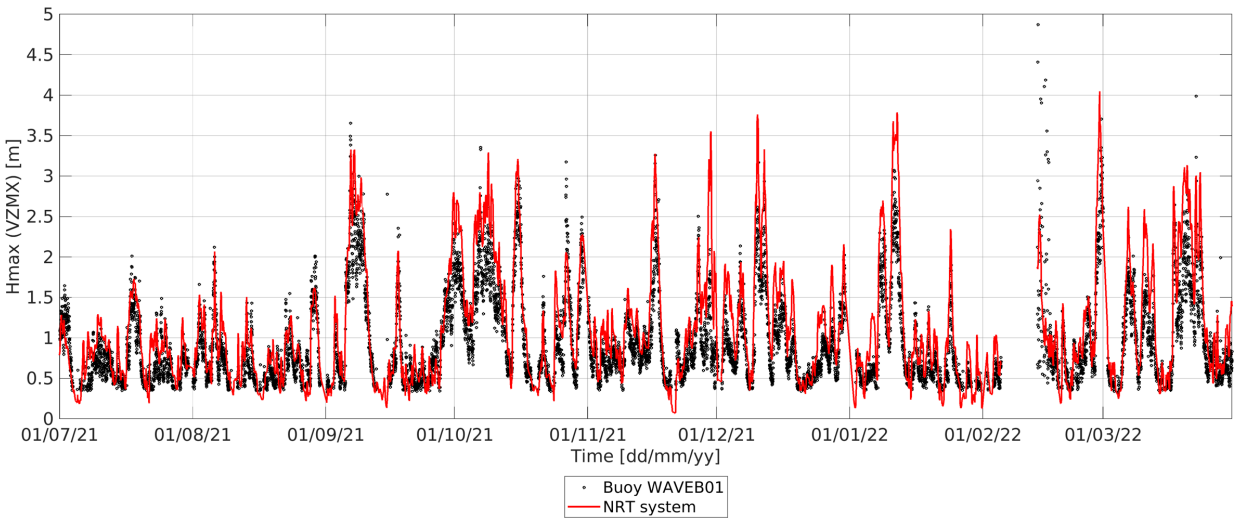

Figure 14: Maximum wave height (VZMX) of the buoy WAVEB01 (all available data). Hmax is not available for WAVEB03; instead WAVEB01 is shown.

When taking into account all buoys and all available buoy data for the considered period, the bias and RMSD of significant weight are 12 and 21 cm, respectively (Table 4). As buoy data is not assimilated into the model, these metrics are good values and also other variables like VTM02, VTPK, VMDR, and VPED show relatively slight deviations from the measurements. Only VZMX shows lower performance.

Although the model-buoy comparisons reveal good model skills, it is noteworthy that the buoy data contain periods with possibly reduced data quality. Especially, the wave directions could be influenced by unprecise calibrations. As noted earlier, we established a collaboration with INS TAC to report measurement issues.

*Table 4: Overall metrics for the NRT BS-waves system using all **buoys**.*

Period: May 2020 to April 2022		
Variable	Bias [cm]	RMSD [cm]
VHM0	12 cm	21 cm
VZMX	18 cm	41 cm
VTM02	-0.3 s	0.9 s
VTPK	0.0 s	1.3 s
VMDR	7°	56°
VPED	-13°	60°

IV.4 Wind assessments

The wind forcing is the most important forcing of the wave model. Thus, it is of utmost importance to determine its quality. Since systematic in-situ measurements of wind in the Black Sea are lacking, the validation is restricted to satellite-obtained wind speed. This quantity is available via CMEMS from February 2020 ongoing for the satellites SARAL/Altika, Cryosat-2, Jason-3, Sentinel-3a, Sentinel-3b, and Sentinel-6a (the same as for significant wave height except CFOSat). The assessment approach is the same as for the SWH (see Figure 5). The comparisons are shown separately for each satellite (Figure 15) as well as for all satellite data merged (Figure 16, left panel). The wind forcing slightly overestimates the moderate winds whereas the low and high winds are represented quite well (see the qq-plot and the diagonal). Very high winds (>~12 m/s) tend to be too low in the forcing. The data of all satellites are quite close to the y-x line and the qq-plots show relatively low deviations of from the diagonal resulting in biases of -0.05 to 0.36 m/s (subfigures of Figure 15). The RMSD ranges from 1.40 to 1.57 m/s with a SI of 0.21 to 0.25. The CORR is relatively constant with values of 0.80 to 0.86. For all satellites together (Figure 16, left panel), the respective values are: bias = 0.22 m/s, RMSD = 1.47 m/s, SI = 0.23, and CORR = 0.84. The distribution of occurrences of specific ranges of wind speed is also in good agreement and shows only slight deviations (Figure 16, right panel). Specifically, the range 3 to 6 m/s in the wind forcing occurs less in compared to the satellite data. However, it is noted that this underrepresented range does not induce an underestimation of the winds (Figure 16, left panel). In summary, the quality of the wind forcing can be considered as good. However, the wind direction is not taken into account is still an unverified error source.

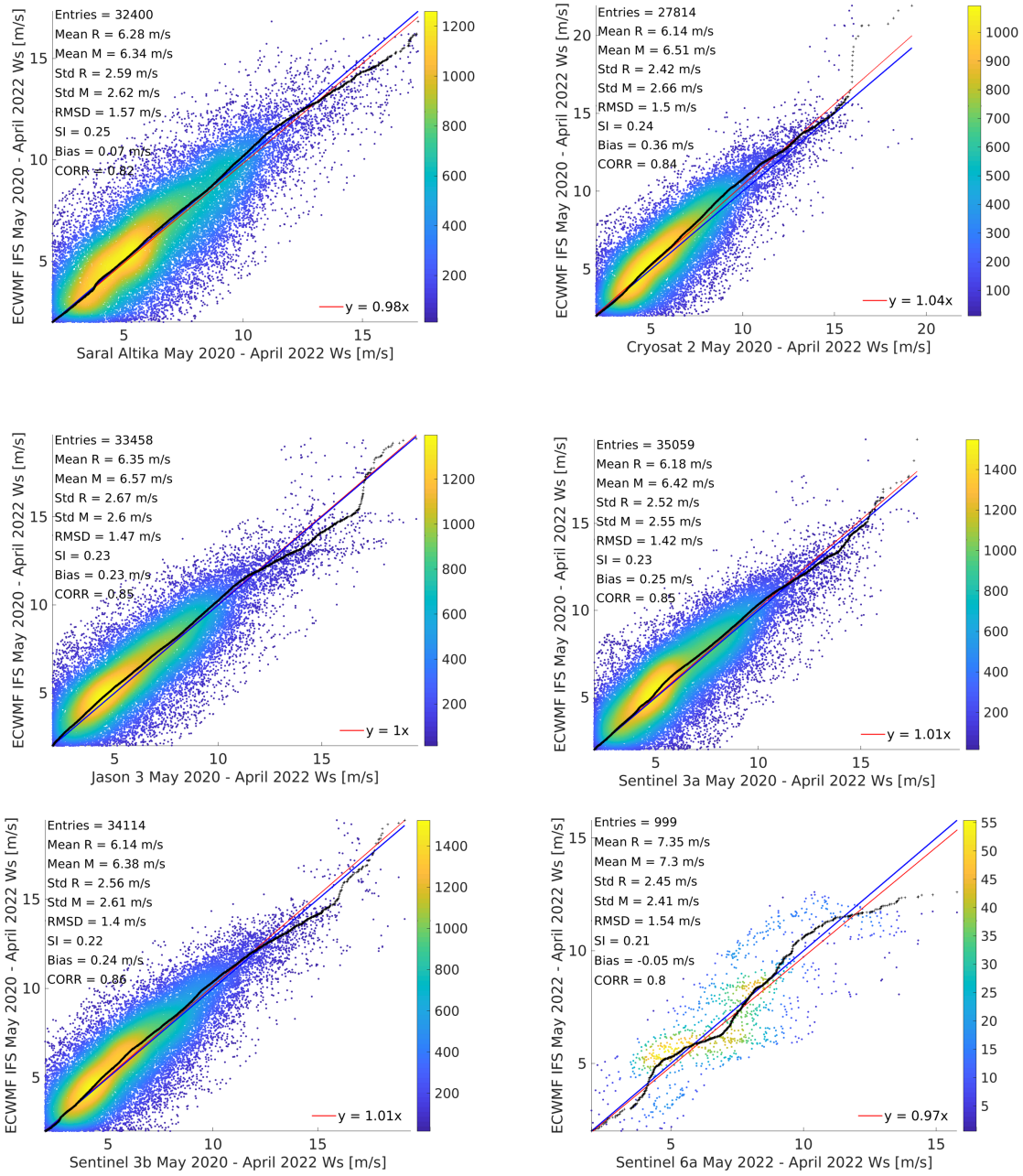

Figure 15: Scatter plots of wind speed obtained from 6 different satellites for the period May 2020 to April 2022 (same as in Figure 5 but without CFOSat). See the labels for the satellite names and Figure 5 for a detailed description of the scatter plots.

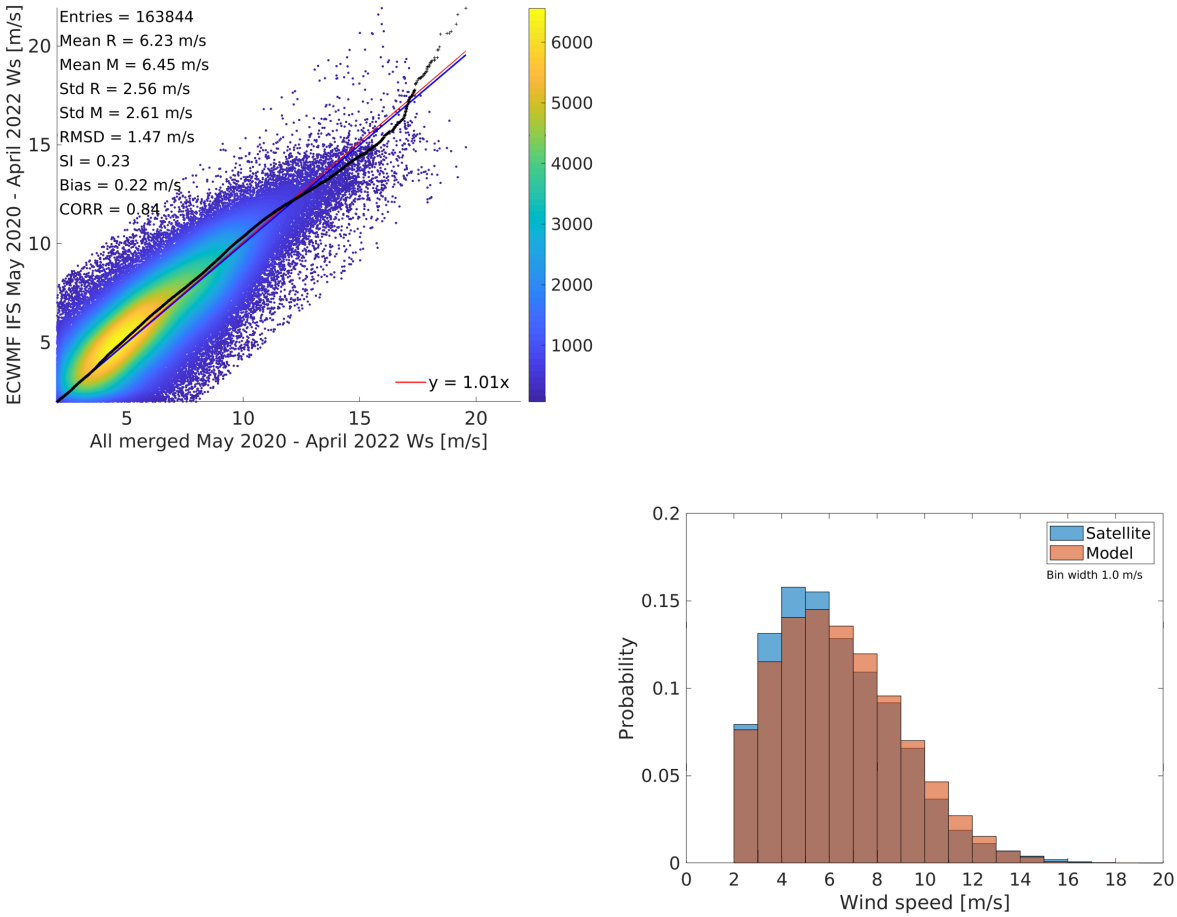

Figure 16: Scatter plot of wind speed obtained from the satellites Jason-3, Sentinel-3a/3b, SARAL/Altika, Cryosat-2, and Sentinel-6a for the period February 2020 to May 2021 (left). Histogram of the scatter plot (right). See Figure 5 for a detailed description of the scatter plot.

IV.5 Mean state

Beyond the discussions concerning the along-track validation and the general statistics in the previous chapters, it is interesting to have a look at the mean of the significant wave heights and the corresponding statistics. Figure 17 presents the mean (upper left), 99th percentile (upper right), the maximum (lower left), and the standard deviation (std) (lower right) of the significant wave height for the 2-year period May 2021 to April 2022. The mean ranges between 0.8 m in the east and 1.2 m in the west. The 99th percentile reaches 3.5 m but has often values of around 3 m. The maximum significant wave height during the 2-year period was ~9 m. The standard deviation ranges between 0.6 and 0.7 m. It is interesting to note that the related coefficient of variation (std/mean) has a relatively uniform value of 0.6, which reveals a high wave variability with respect to the mean.

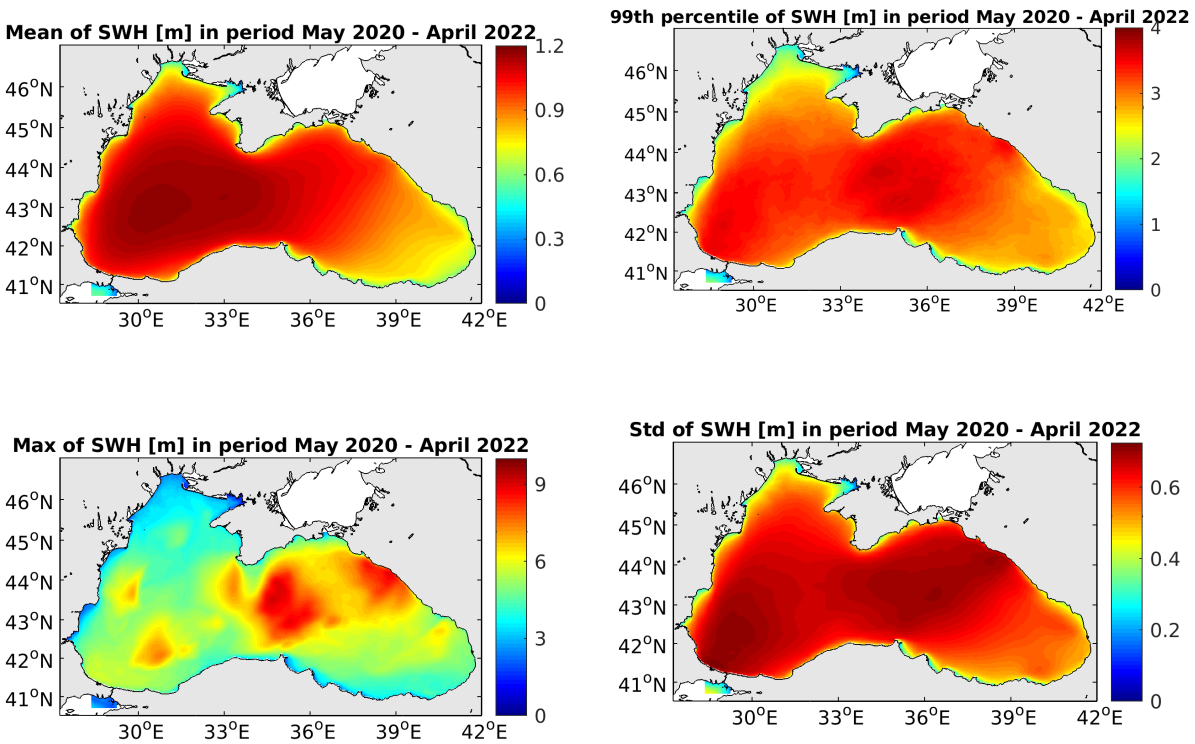

Figure 17: Mean significant wave height (SWH) (top left), 99th percentile of SWH (top right), maximum SWH (lower left), and standard deviation of SWH (lower right) for the period May 2020 to April 2022 obtained from hindcast data.

In the last example of this chapter, Figure 18 demonstrates the temporal evolution of the monthly and spatially averaged mean significant wave height for the complete 2-year period from May 2020 to April 2022 (red solid line). In addition, the monthly means of along-track satellite data (blue dashed line) and the corresponding model values (red dashed line) are shown. The progression of the corresponding curves shows significant differences for the 24 months. At the beginning and at the end of the 2-year period the mean wave height is very small with values between 0.8 and 1.1 m, while the wave heights subsequently increase significantly from August 2020 to January 2021 with a value of 1.3 m as the maximum. Then the curve goes down and up again for a second peak in January 2022 of around 1.6 m, before it decreases again to the end of the period. Considering the differences of the model and satellite along-track curves, is turns out that that the model overestimates the satellite data of about 5 cm but the shape and timing of both curves are almost identical. The corresponding wind time series reveals a clear dependence of the significant wave height on wind speed (Figure 19). Furthermore, the wind is also overestimated by ERA5 (~40 cm/s), at least until September 2021. Accordingly, the SWH differences

also decrease from thereon. This reveals a dependence of SWH overestimation on overestimated winds. In summary, the results of Figures 17-19 show the well-known wave characteristics of the Black Sea and further confirm the model reliability.

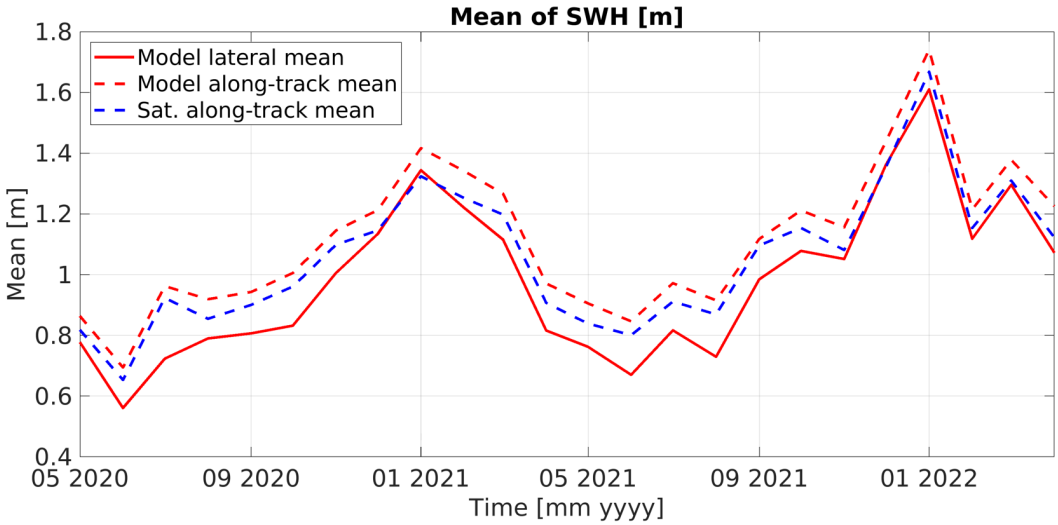

Figure 18: Temporal evolution of monthly and spatially averaged mean significant wave height (SWH) over the period May 2020 to April 2022 (red solid line). In addition, along-track satellite data (blue dashed line) as well as the corresponding model data (red dashed line) are shown.

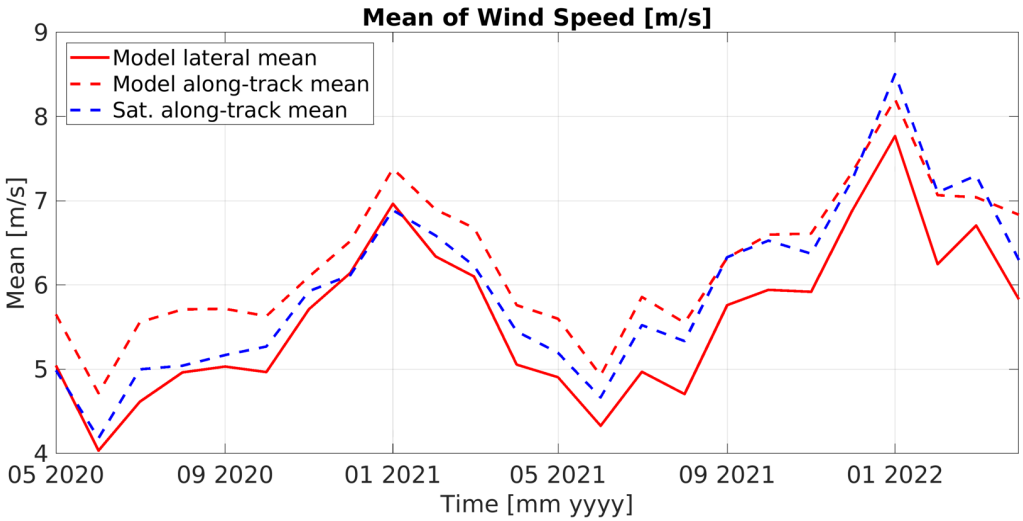

Figure 19: Temporal evolution of monthly and spatially averaged mean wind speed over the period May 2020 to April 2022 (red solid line). In addition, along-track satellite data (blue dashed line) as well as the corresponding model data (red dashed line) are shown.

V SYSTEM'S NOTICEABLE EVENTS, OUTAGES OR CHANGES

The old NRT product BLKSEA_ANALYSISFORECAST_WAV_007_003 will be replaced by the new version of BLKSEA_ANALYSISFORECAST_WAV_007_003 in November 2022.

Date	Change	Notes
Apr 2018	Release of product	
Feb 2019	Changes to reduce underestimation of satellite radar altimetry by model (wave growth parametrisation in wind input source term).	
Dec 2020	NRT system replaced (007_003), changed name ANALYSIS_FORECAST to ANALYSISFORECAST	
Dec 2021	NRT system replaced (new bathymetry and horizontal resolution, new wind forcing).	
Nov 2022	NRT system replaced (addition of data assimilation, new wave model physics - ST4).	

VI QUALITY CHANGES SINCE PREVIOUS VERSION

This section analyses the new BLKSEA_ANALYSISFORECAST_WAV_007_003 product with respect to its previous version BLKSEA_ANALYSISFORECAST_WAV_007_003.

Figure 20 shows comparisons of along-track validations of the new system (left panels) and the old system (right panels) with a descending Cryosat-2 track from 11/03/2021 09:56:32 – 09:57:24 UTC. The presented period shows a storm situation in the north-western part of the Black Sea with significant wave heights up to 3.7 m. In the basin interior, differences between the two systems are hardly noticeable. However, at both the northern and southern coasts distinct improvements are visible. A second example (Figure 21) shows an ascending track of CFOSat passing a storm area in the western basin from 15/12/2021 16:31:15 – 16:32:27 UTC. This comparison reveals a model improve over almost the full period of the track. See also Figure 3 for the description of the new product.

Figure 22 shows a comparison of the statistics between the results of the new system (left panel) and the previous system (right panel) of the wave model by merging all satellite data available for the full period May 2020 to April 2022. All statistical metrics have considerably improved. The bias has improved from -16 to 6 cm, the RMSD from 28 to 13 cm, the SI from 0.22 to 0.10, and the correlation from 0.93 to 0.98. The EANs of the previous system are given in Table 5. It is noted that is partly due to data assimilation.

In the case of wave buoys, the differences between the new and old products are less obvious; especially in the time series. Figure 23 shows the WAVEB03 buoy time series (see also the description of Figure 8 and Table 4) in which almost no changes are visible. However, when taking into account all buoys and the full available periods, the overall metrics (Table 6) and the scatter plots (Figure 24) reveal a model performance improvement only for the T_{m02} and peak periods. The T_{m02} period shows an increase of the short and medium periods, which are now closer at the x-y line. The wave height and direction metrics actually worsend. Especially the wave heights are negatively affected, which are now slightly overestimated. However, this is not necessarily related to a model performance decrease considering the known issues related to the buoys, which are, e.g., their vicinity to the coasts, unknown data quality, unknown coastal wind quality, and a possible unfavourable bathymetry at the buoy locations. These aspects can distort the buoy validations. Furthermore, direct comparisons of satellite and buoy data are currently not possible. It is also highlighted that the new model parameterisations were done with (not assimilated) satellite data, which are still expected to be more reliable considering the amount of measurements and the vast coverage of the domain.

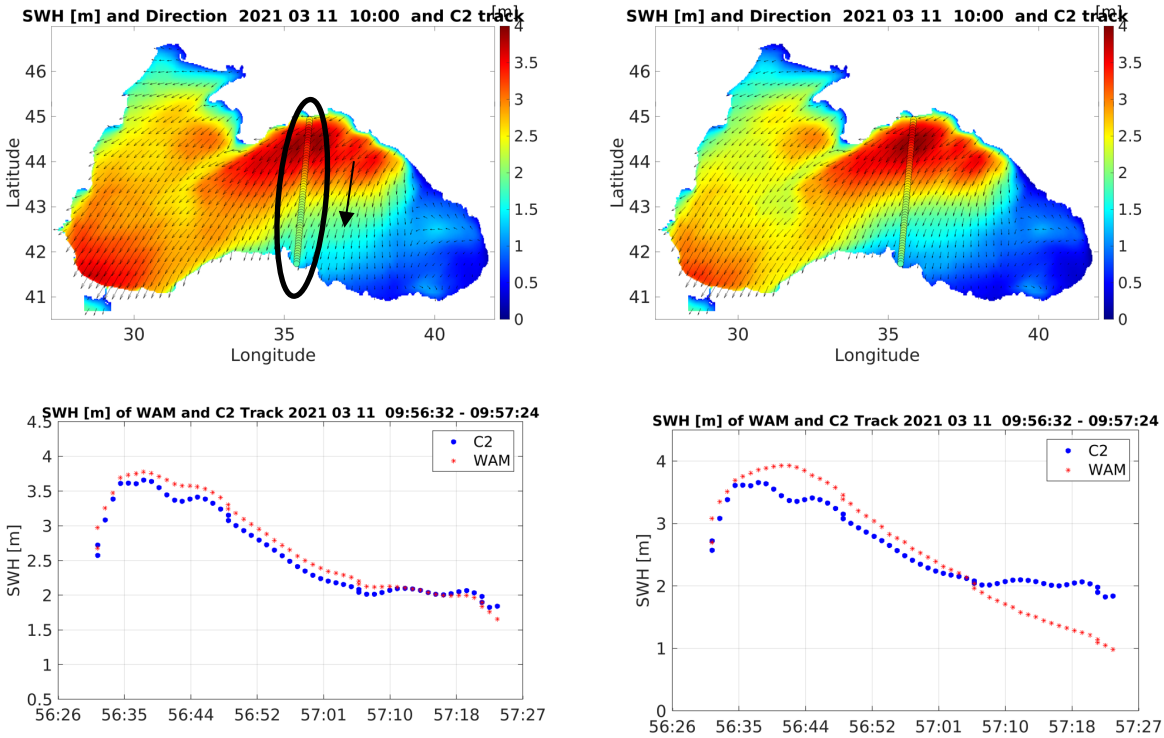

Figure 20: Significant wave height (SWH) satellite along-track comparison of the new product (left) and the old product (right) using the satellite Cryosat-2. Details are given in the labels. Solid black circle: locations of the tracks. Arrow denote the satellite flight direction.

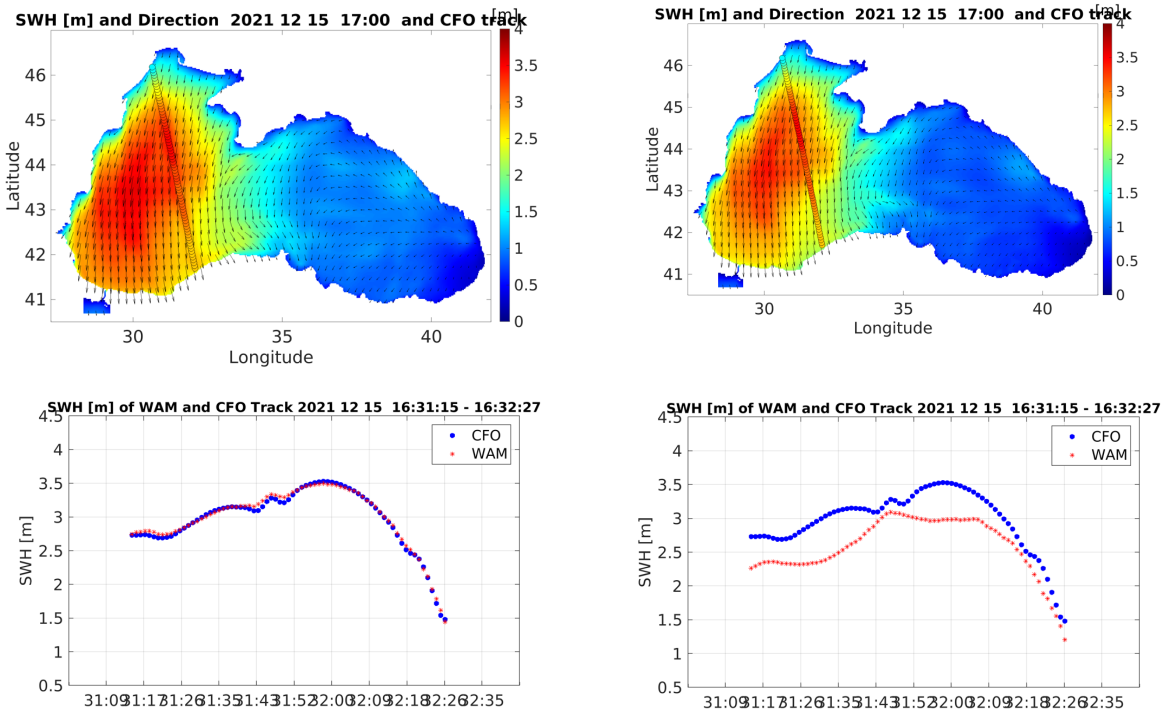

Figure 21: Same as Figure 20 but for the satellite CFOSat.

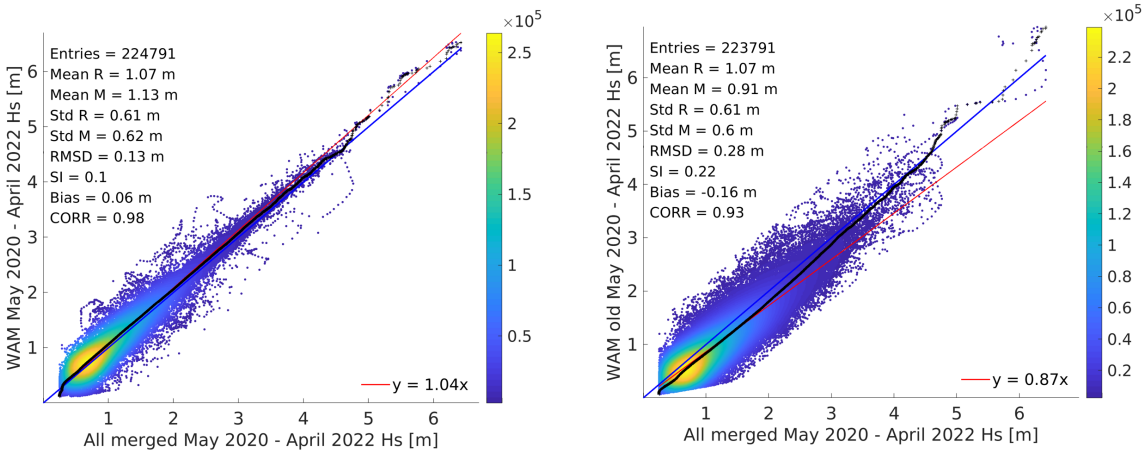

Figure 22: Significant wave height (Hs) scatter plots of the period May 2020 to April 2022 using all satellites merged. Left: new product, right: old product. See Figure 5 for a detailed description of the scatter plots.

Table 5: Significant wave height EANs for the previous NRT BS-waves system and the new one (in brackets) (all values in centimetres).

	June 2019 to May 2021	
	bias	RMSD
All satellites (All merged)	-16 (6)	28 (13)

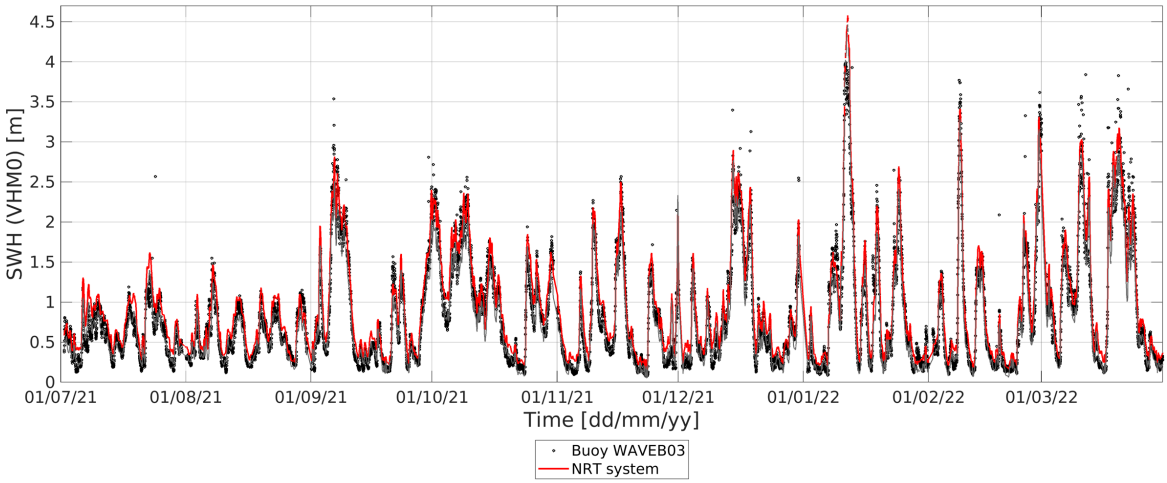

Figure 23: Time series of significant wave height (VHM0) obtained from the buoy WAVEB03. The buoy location can be found in Figure 7. The red line indicates the new product; the thin grey line the old product.

Table 6: Overall metrics using all buoys for the previous NRT BS-waves system and the new one (in brackets).

Period: May 2020 to April 2022		
Variable	Bias [cm]	RMSD [cm]
VHM0	-3 cm (12 cm)	16 cm (21 cm)
VZMX	8 cm (18 cm)	35 cm (41 cm)
VTM02	-0.5 s (-0.3 s)	1.0 s (0.9 s)
VTPK	-0.3 s (0.0 s)	1.4 s (1.3 s)
VMDR	1° (7°)	60° (56°)
VPED	7 (-13°)	60 (60°)

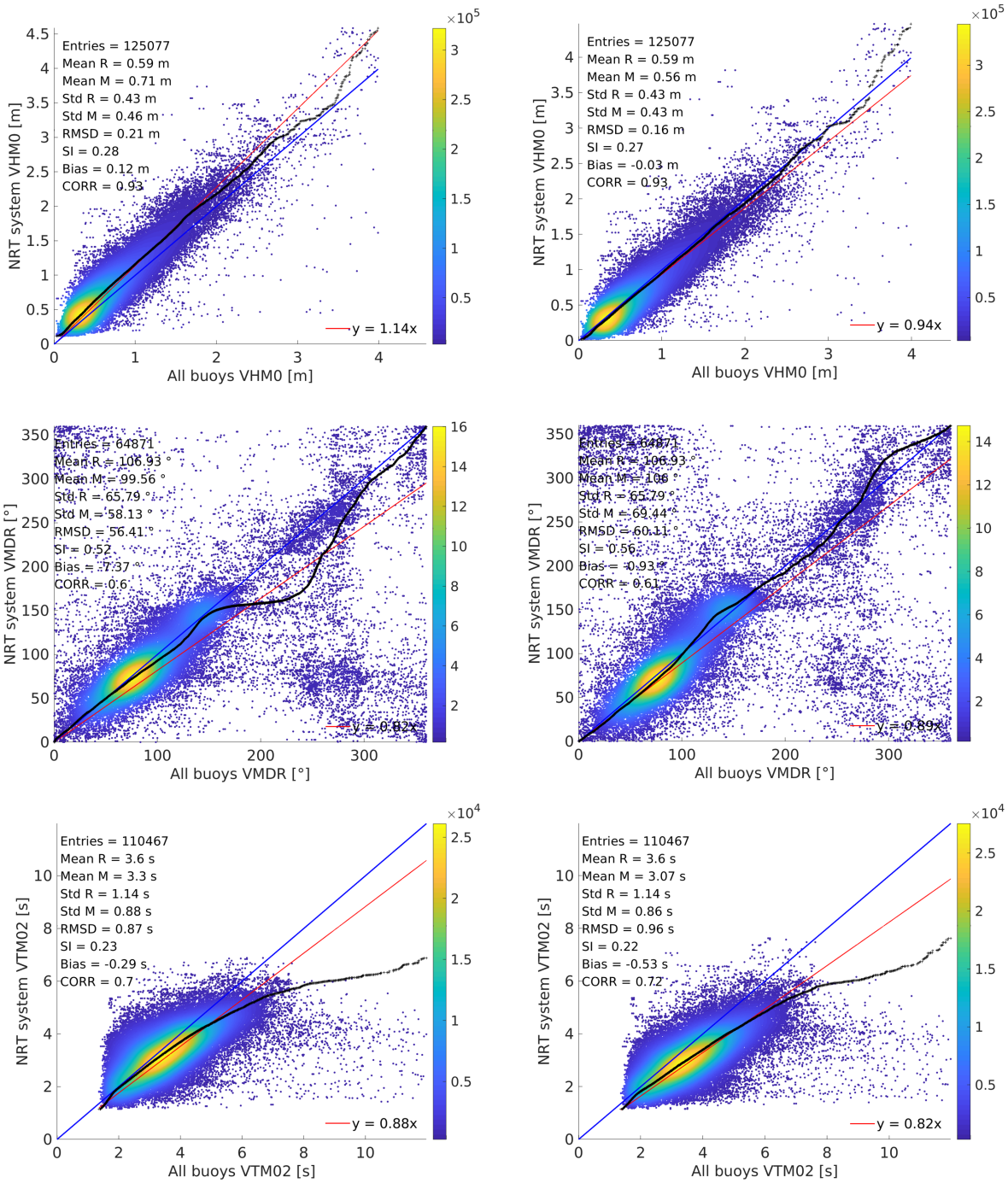

Figure 24: Scatter plots of significant wave height (VHM0), mean direction (VMDR), and T_{m02} period (VTM02) of all wave buoys merged vs. model for the full periods of available buoy data. Left panels: new product, right panels: old product. See Figure 5 for a detailed description of the scatter plots.

VII REFERENCES

Ardhuin, F., Rogers, E., Babanin, A. V., Filipot, J.-F., Magne, R., Roland, A., Westhuysen, A. van der, Queffeulou, P., Lefevre, J.-M., Aouf, L., & Collard, F. (2010). Semiempirical Dissipation Source Functions for Ocean Waves. Part I: Definition, Calibration, and Validation. Journal of Physical Oceanography, 40(9), 1917–1941. https://doi.org/10.1175/2010JPO4324.1

ECMWF (2020) *IFS Documentation CY47R1*, Book Chapter, ECMWF.

Günther, H., Hasselmann, S., Janssen, P. A. E. M. (1992). *The WAM Model Cycle 4.0*. User Manual. Technical Report No. 4, Deutsches Klimarechenzentrum, Hamburg, Germany. 102 pages.

Janssen, P. A. E. M. (1991). Quasi-linear Theory of Wind-Wave Generation Applied to Wave Forecasting. *Journal of Physical Oceanography*, 21(11), 1631-1642. https://doi.org/ 10.1175/1520-0485(1991)021<1631:QLTOWW>2.0.CO;2

Janssen, P. A. E. M. (2008). Progress in ocean wave forecasting. *Journal of Computational Physics*, 227(7), 3572-3594. https://doi.org/10.1016/j.jcp.2007.04.029

Komen, G. J., Cavaleri, L., Donelan, M., Hasselmann, K., Hasselmann, S., & Janssen, P. A. E. M. (1994). *Dynamics and Modelling of Ocean Waves*, Cambridge University Press. https://doi.org/10.1017/CBO9780511628955

Stanev, E. V., He, Y., Staneva, J., & Yakushev, E. (2014). Mixing in the Black Sea detected from the temporal and spatial variability of oxygen and sulfide – Argo float observations and numerical modelling. *Biogeosciences*, 11, 5707–5732. https://doi.org/10.5194/bg-11-5707-2014

Staneva, J., Behrens, A., & Wahle, K. (2015). Wave modelling for the German Bight coastal-ocean predicting system, *Journal of Physics: Conference Series*, 633, 012117. https://doi.org/10.1088/1742-6596/633/1/012117

Staneva, J., Alari, V., Breivik, O., Bidlot, J.-R., & Mogensen, K. (2016a). Effects of wave-induced forcing on a circulation model of the North Sea. *Ocean Dynamics*, 67, 81-101. https://doi.org/10.1007/s10236-016-1009-0

Staneva, J., Wahle, K., Koch, W., Behrens, A., Fenoglio-Marc, L., & Stanev, E. (2016b). Coastal flooding: impact of waves on storm surge during extremes – a case study for the German Bight, *Natural Hazards and Earth System Sciences*, 16, 2373-2389. https://doi.org/10.5194/nhess-16-2373-2016

von Schuckmann, K. et al. (2020). Copernicus Marine Service Ocean State Report, Issue 4. Journal of Operational Oceanography, 13(sup1), S1–S172. https://doi.org/10.1080/1755876X.2020.1785097

von Schuckmann, K. et al. (2021). The CMEMS Ocean State Report, issue 5, Journal of Operational Oceanography, 14:sup1, s1–s185; DOI: 10.1080/1755876X.2021.1946240

Wahle K., Staneva, J., & Günther, H. (2015). Data assimilation of ocean wind waves using Neural Networks. A case study for the German Bight, Ocean Modelling, 96, 117-125. https://doi.org/10.1016/j.ocemod.2015.07.007

WAMDI Group (1988) The WAM model - A third generation ocean wave prediction model. *Journal of Physical Oceanography*, 18(12), 1775-1810. https://doi.org/10.1175/1520-0485(1988)018<1775:TWMTGO>2.0.CO;2